Photoinduced Electron Transfer and Geminate Recombination in Liquids

Kristin Weidemaier, H. L. Tavernier, S. F. Swallen, and M. D. Fayer*

Department of Chemistry, Stanford University, Stanford, California 94305

Received: September 26, 1996; In Final Form: December 19, 1996[⊗]

The coupled processes of intermolecular photoinduced forward electron transfer and geminate recombination between donors (rubrene) and acceptors (duroquinone) are studied in two molecular liquids: dibutyl phthalate and diethyl sebacate. Time-correlated single-photon counting and fluorescence yield measurements give information about the depletion of the donor excited state due to forward transfer, while pump−probe experiments give direct information about the radical survival kinetics. A straightforward procedure is presented for removing contributions from excited-state−excited-state absorption to the pump−probe data. The data are analyzed with a previously presented model that includes solvent structure and hydrodynamic effects in a detailed theory of through-solvent electron transfer. Models that neglect these effects are incapable of describing the data. When a detailed description of solvent effects is included in the theory, agreement with the experimental results is obtained. Forward electron transfer is well-described with a classical Marcus form of the rate equation, though the precise values of the rate parameters depend on the details of the solvents' radial distribution function. The additional experimental results presented here permit a more accurate determination of the forward transfer parameters than those presented previously.[1] The geminate recombination (back transfer) data are highly inverted and cannot be analyzed with a classical Marcus expression. Good fits are instead obtained with an exponential distance dependence model of the rate constant and also with a more detailed semiclassical treatment suggested by Jortner.[2] Analysis of the pump−probe data, however, suggests that the geminate recombination cannot be described with a single solvent dielectric constant. Rather, a time-dependent dielectric constant is required to properly account for diffusion occurring in a time-varying Coulomb potential. A model using a longitudinal dielectric relaxation time is presented. Additionally, previously reported theoretical results[3] are rederived in a general form that permits important physical effects to be included more rigorously.

I. Introduction

The transfer of an electron from a donor to an acceptor is the fundamental step in a wide range of chemical processes. As a result, electron transfer reactions have been the focus of numerous theoretical and experimental efforts aimed at understanding the kinetics and mechanism of the transfer event. One of the great successes has been the Marcus/Hush theory which has provided a quantitative basis for calculating transfer rates since its advent in the 1950s.[4−6] Since then, theoretical advances have gone hand in hand with increasing experimental evidence, so that today the field of electron transfer is central to many areas of protein chemistry, liquid dynamics, and surface science.[7−16]

Despite numerous advances, many key aspects of electron transfer dynamics remain poorly understood. For example, although much effort has been devoted to determining electron transfer rates between covalently bonded species,[8,11,13,14,17−21] fewer studies have been performed on nonbonded donor/acceptor systems. In liquids, nonbonded donor/acceptor systems present a difficult statistical mechanics problem, chiefly because electron transfer from a donor can occur to any of a number of noncontact acceptors, all of which are undergoing diffusional motion. Furthermore, forward electron transfer in liquids is often followed by back transfer (geminate recombination), and the dynamics of the geminate recombination depend strongly on those of the forward transfer.

Historically, models of reaction dynamics in liquids have tended to assume that reaction can occur only when the reacting species are in van der Waals contact.[22] Somewhat more general are treatments that have permitted reaction within a certain radius about the donor.[22−24] When the reactants approach closer than this distance, or Smoluchowski radius, reaction occurs with some rate constant, k. The rate constant and radius of reaction can be treated as adjustable parameters.[22,24] However, for photoinduced electron transfer, while such models have in certain cases provided good fits to experimental data, they also provide limited physical insight.[25−27] It seems clear that a Smoluchowski radius does not correspond to a real physical distance in a liquid; nor is it likely that reaction within this radius should be well described by a single rate constant. Such distance-independent electron transfer rates are inconsistent with a Marcus form of the transfer rate[4] as well as other theoretical descriptions of distance-dependent electron transfer.[28−30]

More sophisticated treatments of reaction kinetics in liquids have been available for a number of years. Tachiya, for example, described rigorously the case of reaction in liquids for any distance-dependent form of the rate constant, $k(R)$, with the diffusion of the particles appropriately included.[31] (Application of such a theory, as will be discussed later, requires input of an appropriate initial spatial distribution, which can be a difficult problem.) His result has been used to describe forward electron transfer without the need for approximations such as the Smoluchowski and Collins Kimball model.[32−34] The complementary problem of back electron transfer (geminate recombination), however, has only recently been treated with a corresponding degree of theoretical rigor.[35] This is due to an inherent complexity arising from the coupled forward and back transfer dynamics. Unlike the forward transfer problem, where the initial distribution of acceptors about the donor can be assumed to be an equilibrium one, the back transfer has initial

[⊗] Abstract published in *Advance ACS Abstracts,* February 15, 1997.

S1089-5639(96)02973-8 CCC: $14.00

conditions that cannot be known *a priori*. That is, the spatial distribution of donor and acceptor ions that will undergo recombination is determined by the details of the forward electron transfer. This couples the differential equations in a nontrivial way. Numerous simplifying approximations have been suggested that either assume that transfer occurs only to a single acceptor or else impose some additional requirement about the spatial arrangement of ions about the donor. However, these approximations have been shown to be inaccurate for all but the lowest acceptor concentrations.[36−38] Recently, a rigorous treatment for the coupled forward and back electron transfer reactions in liquids has been presented.[35] This treatment properly accounts for the full spatial dependence of the problem. Forward transfer can occur through-space from the donor to any of the acceptors, and the kinetics of the geminate recombination depend explicitly on where the ions were initially created, *i.e.* on the details of the forward transfer. It should be stressed that the significance of the recent theoretical developments[39,40] is that they provide the general ensemble averaging techniques needed to handle electron transfer in liquids when more than one acceptor can be involved in the transfer. For real liquids, at all reasonable acceptor concentrations, it is essential to include the full distance dependence of the problem and the rigorous coupling between the forward and back transfer.

Although the methods for performing the ensemble averaging for intermolecular electron transfer in liquids are quite general, the original presentation of these results made no attempt to include certain essential microscopic features of the liquid structure. In two recent publications,[1,3] however, it was shown that inclusion of such effects is crucial to any meaningful analysis of electron transfer in liquids. To assume that the solvent can be well described by a featureless continuum is to introduce serious errors of both a qualitative and quantitative nature. Rather, solvent structure must be explicitly included in the theory through an appropriate radial distribution function, $g(R)$. The radial distribution function affects the dynamics in two ways. First, it leads to a significant increase in the amount of short time electron transfer. This arises because the concentration of acceptors within the first solvent shell is greater than the average concentration that occurs in a continuum model. Second, the radial distribution function acts as an effective potential in which diffusion occurs. Hence, acceptors within the first solvent shell will experience difficulty escaping from the solvent cage, just as more distant acceptors will have difficulty diffusing into the first solvent shell. Although the existence of solvent structure and its description via a pair distribution function is well-known, it is only very recently that such effects have been included in a rigorous treatment of intermolecular electron transfer in liquids.[1,3] Finally, in addition to a pair distribution function, real solvents will also exhibit a so-called hydrodynamic effect, *i.e.*, a distance-dependent diffusion constant. As the donors and acceptors diffuse together, their rate of approach is limited by the speed at which solvent molecules can be "squeezed" out of the intervening space. This becomes more difficult to do at small donor−acceptor distances, and the rate of donor−acceptor mutual diffusion becomes much slower at small distances. This decreases the rate of electron transfer at longer times compared to a standard treatment in which the diffusion constant is distance independent. A complete discussion of these microscopic effects has been given elsewhere,[1,3,22,41,42] and the reader is referred to the references for the details.

This paper serves as the third in a series of publications that treat solvent structural and hydrodynamic effects in intermolecular electron transfer in liquids. In ref 3, the key theoretical results were developed, and illustrative calculations were presented to demonstrate the dramatic influence of solvent effects on the transfer dynamics. In ref 1, experimental results were presented for forward electron transfer between a donor (rubrene) and an acceptor (duroquinone) in various solvents. This reference gave a preliminary analysis of forward transfer data, using the new theory and demonstrating that the molecular rate parameters from the data analysis depend critically on proper inclusion of solvent effects. The current paper treats the question of geminate recombination. Its purpose is 2-fold. Primarily, it presents complete data on the combined forward and back electron transfer dynamics of rubrene and duroquinone in two different solvents. A substantial amount of new data is presented. Two-color pump−probe experiments are used to probe the ion dynamics, giving direct information on ion survival times. Additionally, single-color pump−probe experiments provide information on ground-state recovery. These results, combined with the time-correlated single-photon-counting data presented in ref 1, provide a complete description of the coupled forward and back electron transfer dynamics. New fluorescence yield measurements also give insight into the short time dynamics. Both the forward and back transfer dynamics are analyzed with a detailed theory that includes solvent structure and hydrodynamic effects. It is demonstrated that for both the forward transfer and the geminate recombination, inclusion of these solvent effects is critical for a physically realistic description of the system. Furthermore, it is shown how a set of combined forward and back transfer experiments gives direct information that cannot be obtained by studying either process in isolation. The results suggest another consideration important for the analysis of electron transfer in liquids**:** a time-dependent dielectric constant may be critical for a proper description of the geminate recombination of ions. Finally, this work serves the additional purpose of summarizing the key theoretical results in a compact form suitable for use by experimentalists working in the field. Aspects of the theory are rederived in a more general form, and some new theoretical considerations are presented.

II. Theory

The model system for photoinduced intermolecular electron transfer in liquids has been described in detail elsewhere.[1,3] Upon photoexcitation, the donors can undergo forward electron transfer through-solvent to one of the many acceptors in solution. The donor concentration is kept low ($\sim 10^{-4}$ M) to avoid donor−donor excitation transfer. The acceptor concentration (0.1−0.4 M) is much higher than the donor concentration, so that each donor sees an ensemble of possible electron acceptors. Which acceptor receives the electron depends on the spatial distribution of acceptors about the excited donors and on the nature of molecular diffusion in the liquid. While the theoretical treatment is general for any initial charges on the donors and acceptors, in the study presented below, the forward electron transfer results in the formation of a donor cation and an acceptor anion diffusing in the resulting Coulomb potential. If the ions are initially formed at large separations and if the shielding due to the solvent is strong, the ions can diffuse far enough apart to effectively escape recombination. In the more likely scenario, the electron will back transfer from the acceptor anion to the donor cation, regenerating the ground state. Because the concentration of donors is low, only geminate recombination is considered. Processes that regenerate the donor excited state are energetically unfavorable for the systems studied here and are assumed to be negligible because of the very rapid geminate recombination.[43] The three-level system (consisting only of

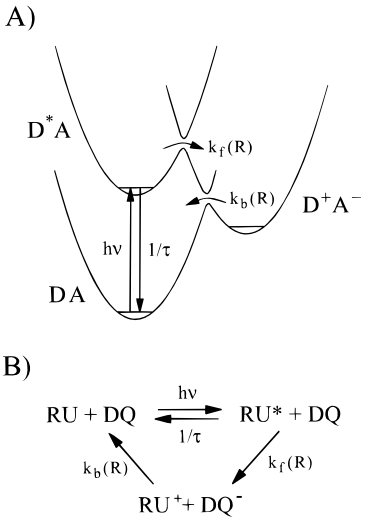

Figure 1. (A) Three-level system consisting of a neutral donor in its ground electronic state and any number of neutral acceptors (DA), excited donor and any number of neutral acceptors (D*A), and radical state, in this case a donor cation and an acceptor anion (D^+A^-). (B) Schematic of the coupled forward and back transfer processes. The donor is rubrene (RU) and the acceptor is duroquinone (DQ). Depletion of RU* is monitored by TCSPC and fluorescence yield experiments, while pump−probe measurements give the RU^+ kinetics.

ground states, excited donor states, and ion states) is shown schematically in Figure 1. Experimental results presented below indicate that the formation of triplets is not involved in the kinetics.

The key goal of the theory is to permit calculation of the physical observables: the state survival probabilities $\langle P_{ex}(t)\rangle$ and $\langle P_{ct}(t)\rangle$. If the donor is photoexcited at time 0, then $\langle P_{ex}(t)\rangle$ is the probability that the donor is still excited at some later time t, while $\langle P_{ct}(t)\rangle$ is the time-dependent probability that the radicals formed by forward transfer still exist. As time evolves, the probability of the donor remaining excited, $\langle P_{ex}(t)\rangle$, decays due to forward electron transfer. While $\langle P_{ex}(t)\rangle$ decays from a value of 1.0 (unit probability at time 0), $\langle P_{ct}(t)\rangle$, the probability of finding the donor and acceptor in their radical states, builds up from 0 as forward transfer occurs and then decays as back transfer acts to deplete the radical population. The ensemble-averaging techniques relate the observables to the two-particle survival probabilities. For the forward transfer,$\langle P_{ex}(t)\rangle$ has been derived in detail elsewhere.[3,31] The result is

$$\langle P_{ex}(t)\rangle = \exp(-t/\tau)\exp(-4\pi C\int_{R_m}^{\infty}[1 - S_{ex}(t|R_0)]R_0^2 g(R_0)\,dR_0) \quad (1)$$

Here, τ, C, and R_m denote respectively the donor fluorescence lifetime, the acceptor concentration, and the donor−acceptor contact distance (sum of their radii). $g(R_0)$ is an appropriate donor/acceptor radial distribution function. $S_{ex}(t|R_0)$ is the two-particle excited-state survival probability, a theoretical construct for a hypothetical system in which there is one donor and only one acceptor. Given that the acceptor is at distance R_0 from the donor at time 0, $S_{ex}(t|R_0)$ is the probability that the donor is still excited at time t later. $S_{ex}(t|R_0)$ satisfies the well-known differential equation, with associated initial condition[23]

$$\frac{\partial}{\partial t}S_{ex}(t|R_0) = L^+_{R_0}S_{ex}(t|R_0) - k_f(R_0)\,S_{ex}(t|R_0) \quad (2)$$

$$S_{ex}(0|R_0) = 1$$

$k_f(R_0)$ is a distance-dependent forward transfer rate, the specification of which is left until section IV. $L^+_{R_0}$ is the adjoint of the Smoluchowski operator:[23,44]

$$L^+_{R_0}0 = \frac{1}{R_0^2}\exp(V(R_0))\frac{\partial}{\partial R_0}D(R_0)R_0^2\exp(-V(R_0))\frac{\partial}{\partial R_0} \quad (3)$$

where $V(R_0)$ is the potential divided by k_BT, and $D(R_0)$ is the distance-dependent diffusion constant. Numerical evaluation of eq 2 can be followed by integration according to eq 1 to give the forward transfer experimental observable. This observable can be directly compared to experimental measurements of the time dependence of donor fluorescence emission using techniques such as time-correlated single-photon counting or fluorescence upconversion.

The inclusion of solvent structure and of a distance-dependent diffusion constant (hydrodynamic effect) in eqs 1−3 has been discussed previously.[3] The radial distribution function, $g(R_0)$, must appear in both the spatial averaging and in the diffusional operator. In eq 3, the potential in the Smoluchowski operator must include the potential of mean force, *i.e.* $V(R_0) = -\ln[g(R_0)]$. The distance dependence of the diffusion constant also appears within the Smoluchowski operator.

Derivation of the theoretical results for $\langle P_{ct}(t)\rangle$, as already mentioned, requires solving the coupled forward and back transfer problem. The techniques for performing the ensemble averages for the coupled problem have been presented previously[39,40] and were used in ref 3 to include solvent structure and hydrodynamic effects. The result is

$$\langle P_{ct}(t)\rangle = 4\pi C\int_{R_m}^{\infty}\int_0^t S_{ct}(t - t'|R_0)\,k_f(R_0)\,S_{ex}(t'|R_0)\times \langle P_{ex}(t')\rangle\,dt' R_0^2\,g(R_0)\,dR_0 \quad (4)$$

$S_{ct}(t|R_0)$ is the two-particle survival probability for the radicals. That is, given that at time 0 the acceptor exists as a radical at R_0, $S_{ct}(t|R_0)$ is the probability that the donor and acceptors still exist as radicals at time t later; that is, back transfer has not yet occurred. $S_{ct}(t|R_0)$ can be calculated using eq 2 with the appropriate back transfer rate, $k_b(R_0)$, and the potential modified to include the Coulomb potential for radicals that are ions as discussed in the experiments below:

$$V(R_0) = -\ln[g(R_0)] + \frac{Z_DZ_Ae^2}{4\pi\epsilon_0\epsilon_sk_BTR_0} \quad (5)$$

In eq 5, ϵ_0 is the permittivity of free space, e is the unit of fundamental charge, Z_D and Z_A are the charges on the donor and acceptor ions, respectively (in units of e), and k_BT is the Boltzmann constant times the temperature. ϵ_s is the low-frequency (static) dielectric response.

Equation 4 represents the most commonly encountered experimental situation, in which the donor and acceptor have no Coulomb interaction prior to forward electron transfer. Equation 4 also represents the most computationally convenient form for the radical survival probability, $\langle P_{ct}(t)\rangle$, since $S_{ct}(t|R_0)$ satisfies a differential equation equivalent to that of $S_{ex}(t|R_0)$. It should, however, be stressed that while the results presented previously[3] are formally correct for diffusion in a potential of mean force, inclusion of any additional potential in the forward transfer will require modification of the ion survival equations (eq 4). This fact, although not immediately obvious, arises from the need to distinguish formally between the adjoint and nonadjoint forms of the Smoluchowski operator. In the original derivation of $\langle P_{ct}(t)\rangle$ (eq 10 in ref 3 and eq 4 above), it was assumed that the only potential involved in the forward transfer was a potential of mean force, *i.e.* $V(R_0) = -\ln[g(R_0)]$. (This

includes the special, although unphysical, case of $g(R_0) = 1$ everywhere, *i.e.* a featureless solvent.) As long as the only potential between the donor and acceptor prior to forward transfer is the potential of mean force, then for any potential in the back transfer, eq 4 is valid.

In the most general case, however, a potential other than that of mean force might exist between the donor and acceptor prior to forward transfer. The most obvious example would be one in which both donor and acceptor reactants were charged. In this case, eq 4 no longer holds. Instead, as shown in Appendix A, the following equations must be used.

$$\langle P_{ct}(t)\rangle = 4\pi C \int_{R_m}^{\infty}\int_0^t S_{ct}(t - t'|R_0)\, k_f(R_0)\, b_{ex}(R_0,t')\langle P_{ex}(t')\rangle R_0^{\,2}\, dR_0\, dt' \quad (6)$$

where

$$\frac{\partial}{\partial t} b_{ex}(R,t) = L_R b_{ex}(R,t) - k_f(R)\, b_{ex}(R,t) \quad (7)$$

$$L_R = \frac{1}{R^2}\frac{\partial}{\partial R}\left[R^2 D(R)\exp(-V(R))\frac{\partial}{\partial R}[\exp(V(R))]\right]$$

$$b_{ex}(R,0) = g(R)$$

Equations 6 and 7 represent the most general result and are formally valid for any form of the distance-dependent potential, $V(R)$, in the forward or back transfer stages. Equation 4, although valid for any form of the potential between the radical *ions*, requires that there be no potential between the pretransfer donor and acceptors other than a potential of mean force. In all cases, eq 1 for $\langle P_{ex}(t)\rangle$ is valid.

III. Experimental Procedures

The electron transfer system is an optically excited donor, rubrene, undergoing electron transfer to an acceptor, duroquinone, to form the radical cation and anion, respectively. Geminate recombination can then occur. The experiments were conducted in two solvents: dibutyl phthalate and diethyl sebacate. Details of the sample preparation have been given elsewhere.[1] In brief, the solvents were the highest commercial grade available from Aldrich and were used without additional purification. Rubrene and duroquinone were also obtained from Aldrich. The duroquinone was purified by sublimation, while rubrene was dissolved in the degassed solvent and filtered through a 0.2 μm filter. Because rubrene decomposes in the presence of oxygen and light, all samples were prepared by freeze−pump−thawing in evacuable spectroscopic cells. The cells were sealed under ~1 atm of inert gas. Rubrene concentrations were less than 2.0×10^{-4} M, while DQ concentrations were in the range 0.10−0.45 M. All concentrations were determined spectroscopically.

The static dielectric constant for dibutyl phthalate was taken from ref 45. For diethyl sebacate, the dielectric constant is not reported in the literature. However, a value of 4.54 is reported for dibutyl sebacate,[45] and the diethyl sebacate value should be only slightly larger. Capacitance bridge measurements on diethyl sebacate were performed and yielded a dielectric constant of approximately 5. Since the geminate recombination calculations are somewhat sensitive to two significant figures in the dielectric constant, a value of $\epsilon_s = 4.7$ was used for diethyl sebacate to account for a small increase over the dibutyl sebacate literature results.

Cyclic voltammetry measurements were performed on rubrene and duroquinone in both solvents. The measured redox potential difference was used to calculate the free energy change, ΔG_f, for the forward transfer by means of the Rehm−Weller equation.[46,47]

$$\Delta G_f(R) = \xi^0(\text{donor,ox}) - \xi^0(\text{acceptor,red}) - \Delta E - \frac{e^2}{4\pi\epsilon_0\epsilon_s R} \quad (8)$$

where ξ^0(donor,ox) − ξ^0(acceptor,red) is the measured redox difference, and ΔE is the rubrene $S_0,\nu_0 \rightarrow S_1,\nu_0$ excitation energy, taken as 543 nm, the wavelength where the rubrene absorption and fluorescence spectra overlap.[48] The last term in eq 8 is a Coulomb term that depends on the distance between the ions. The free energy change for the back transfer, ΔG_b, was then determined by

$$-\Delta G_b(R) = \Delta E + \Delta G_f(R)$$

Details of the cyclic voltammetry measurements are given in ref 1.

Time-correlated single-photon-counting (TCSPC) experiments were performed to elucidate the kinetics of the forward transfer process. The experimental system has been described previously.[1] A mode-locked Nd:YAG laser was frequency doubled and used to pump a Spectra Physics dye laser tuned to 550 nm with base-shifted Fluorescein 548 dye (Exciton). An acoustooptic cavity dumper provided 10 ps pulses from the dye laser at a repetition rate of 800 kHz. These pulses were attenuated and used for magic angle excitation of the sample. Fluorescence was detected through a vertical polarizer and a dispersive subtractive monochrometer with a Hamamatsu (R2809-06) multiple channel plate detector. Fluorescence detection was performed at several wavelengths, and no wavelength dependence of the decays was observed. The instrument response of the TCSPC system was 50 ps.

Fluorescence yield measurements, like the pump−probe measurements described below, were performed on a different laser system than that used for the TCSPC experiments. An acoustooptically mode-locked and Q-switched Nd:YLF laser provided 3.5 W of 1053 nm light. Half of this was frequency doubled and used to pump a visible dye laser operated with Rhodamine 575 dye obtained from Exciton. Cavity dumping the dye laser with a KD*P Pockels cell gave 10−30 μJ pulses, depending on the wavelength. The fluorescence yield experiments were performed at 550 nm, on the red-edge of the rubrene ground-state absorption spectrum. A sample holder was built to ensure reproducible placement of the samples within the laser beam. After magic angle excitation by the 550 nm pulse, sample fluorescence was collected by a lens, passed through a vertical polarizer, and detected with a photomultiplier tube (PMT). The integrated fluorescence was detected with a lock-in amplifier. The measurements were repeated several times at various laser powers to ensure the absence of intensity artifacts.

Pump−probe measurements were performed with the same laser system used in the fluorescence yield experiments. The remaining portion of the Nd:YLF light was frequency doubled and used to pump a second dye laser tuned to the rubrene cation absorption. A change in laser dye (LDS 867−LDS 925) permitted tuning over a significant region of the near-IR, and pump−probe experiments were performed with probe wavelengths varying between 840 and 980 nm. At all these probe wavelengths, significant ion absorption was observed, in agreement with the published rubrene cation spectrum.[49] However,

the measured kinetics did not depend on the probe wavelength within the time-resolution of the experiment (30 ps).

All pump−probe experiments were performed at the magic angle. A portion of the probe beam picked-off prior to the sample was detected by a reference photodiode. The main probe beam, after passing through the sample, was detected by the signal photodiode. The outputs of both the reference and signal detectors were each sent to gated integrators (SRS). An analog processor (SRS) then divided the output of the signal gated integrator by the output of the reference gated integrator, thereby eliminating shot-to-shot noise in the probe. The analog processor also performed the log of the divided signal, and this log output was detected by a lock-in amplifier. The output of the lock-in is thus a direct measurement of the change in probe absorption induced in the sample by the pump pulse, corrected for probe shot-to-shot fluctuations. The intensities of both the pump and probe beams were reduced until further reduction resulted in no change in the signal, thereby avoiding power artifacts.

Ground-state recovery pump−probe experiments were also performed. The 550 nm beam from the visible dye laser was split by an 80/20 beamsplitter to provide both pump and probe beams.

IV. Data Analysis

The TCSPC experiments, combined with the fluorescence yield measurements, give complete information about the forward transfer dynamics. The time-resolved forward data can be fit with eq 1 to yield information about the intermolecular electron transfer rate, $k_f(R)$. In ref 1, the TCSPC data were presented and analyzed using the well-known Marcus result:[4,5]

$$k_f(R) = \frac{2\pi}{\hbar\sqrt{4\pi\lambda(R)k_B T}} J_{of}^{\,2} \exp\left(\frac{-(\Delta G_f(R) + \lambda(R))^2}{4\lambda(R)k_B T}\right) \times \exp(-\beta_f(R - R_m)) \quad (9a)$$

where

$$\lambda(R) = \frac{e^2}{2}\left(\frac{1}{\epsilon_{op}} - \frac{1}{\epsilon_s}\right)\left(\frac{1}{R_d} + \frac{1}{R_a} - \frac{2}{R}\right) \quad (9b)$$

$\Delta G_f(R)$ is the free energy change for the forward transfer, obtained from the cyclic voltammetry experiments and the Rehm−Weller equation (eq 8). ϵ_{op} and ϵ_s are the optical and static dielectric constants of the solvent, ϵ_0 is the permittivity of free space, and R_d and R_a are the donor and acceptor radii, respectively. Although more sophisticated forms of the rate constant have been suggested,[2,11,29,30,50,51] many of these forms can be approximated by eq 9 in the noninverted regime.[48] Since ΔG_f in the solvents is relatively small for the forward transfer, eq 9 is expected to be accurate. The adjustable parameters are then J_{of} and β_f, which determine the magnitude and distance dependence of the electronic coupling, respectively.

The fluorescence yield measurements presented for the first time in this paper supplement the TCSPC experiments and provide additional insight into the short time dynamics. This additional information stems from the recognition that the fluorescence yield experiments are time-integrated measurements and thus are insensitive to the instrument response. In fitting the time-resolved dynamics, $\langle P_{ex}(t)\rangle$ calculated from eq 1 must be convolved with the instrument response, thereby reducing sensitivity to the short time dynamics. The fluorescence yield experiments, in contrast, are sensitive to the unconvolved $\langle P_{ex}(t)\rangle$. The yield, Φ, is defined:

$$\Phi = \frac{1}{\tau}\int_0^\infty \langle P_{ex}(t)\rangle \, dt \quad (10)$$

The parameters J_{of} and β_f, then, must yield calculations consistent with both the yield data and the time-dependent data. While eq 10 by itself is not sufficient to ensure unique values of J_{of} and β_f, it will eliminate fits to the TCSPC data that do not lead to sufficiently fast decays within the instrument response.

Analysis of the combined fluorescence yield and TCSPC data yields the forward transfer parameters, J_{of} and β_f. Once these parameters are known, the complete time and spatial dependences of the forward kinetics (*i.e.* where and when the radicals were formed) are known. The recombination (back transfer) kinetics can then be probed through an independent set of measurements: the pump−probe experiments. The rubrene cation spectrum has broad-band absorption between 730 and 980 nm.[49] Pump−probe experiments with the probe beam tuned to the rubrene cation absorption should then provide a direct measurement of $\langle P_{ct}(t)\rangle$ for comparison with eq 4. The data analysis, however, was complicated by the presence of a rubrene excited-state−excited-state absorption at the same frequencies as the rubrene cation absorption. Although the probe was tuned over a region of approximately 100 nm, no wavelength could be found at which the excited-state−excited-state contribution was negligible. Thus, instead of directly probing $\langle P_{ct}(t)\rangle$, the experiments measured a linear combination of $\langle P_{ex}(t)\rangle$ and $\langle P_{ct}(t)\rangle$, with the contribution of each determined by the ratio of the absorption coefficients of the excited and radical rubrene states, respectively. Since this ratio is not known, it might be treated as an additional fitting parameter. However, it can be shown that this is not necessary. The contribution to the pump−probe signal from excited-state−excited-state absorption can, in fact, be eliminated *without any knowledge about the absorption coefficients* of either the rubrene ion or the rubrene excited state. This non-obvious result greatly aids in the analysis of the two-color pump−probe data and permits the time dependence of the rubrene cation probability to be extracted directly from the raw experimental data.

The procedure for eliminating the contribution from excited-state absorption (although somewhat tedious) is straightforward, and the details are presented in Appendix B. In essence, the technique relies on knowing the shape of the excited-state contribution from the independent TCSPC experiments. A sample of pure donor in the appropriate solvent can then be used to calibrate the contribution of the rubrene excited state to the pump−probe signal. Accurate measurement of the rubrene absorption of the pump beam is essential. Hence, absorption measurements for all samples were performed directly with the laser excitation beam at the same time as pump−probe data acquisition. Shot-to-shot noise was minimized by dividing the transmitted laser intensity by a reference. Appendix B describes the complete procedure.

Once direct experimental determination of $\langle P_{ex}(t)\rangle$ and $\langle P_{ct}(t)\rangle$ has been made by TCSPC and pump−probe experiments, respectively, the results can be compared to the predictions of eqs 1, 10, and 4. (Note that since the forward transfer involves neutral species, either eqs 4 or 6 can be used to fit the pump−probe data. Equation 4 was selected because of slightly greater numerical ease.) The rate parameters, J_0 and β, can be determined for both the forward and back transfer processes by fits to the experimental data. For meaningful results, the theory must include all relevant information about solvent structure and hydrodynamic effects. Equations 1−7 show how the radial distribution function and distance-dependent diffusion constant should be included in the theory. Accurately determin-

ing $g(R)$ and $D(R)$ for a specific electron transfer system in a particular molecular solvent presents difficulties. A detailed discussion of this issue, along with suggestions on how to determine parameters for a real physical system, is given in ref 1. The key points can be briefly summarized.

First, as reference 1 demonstrated, a hard-sphere $g(R)$ is sufficiently accurate for electron transfer calculations. This is a consequence of the very fast rate of transfer at short distances. Detailed knowledge of the distribution of acceptors about the donor within the first two or three angstroms is not essential. It is sufficient if the radial distribution function predicts the correct short-distance number density.[1] The hard-sphere $g(R)$ can be calculated by standard algorithms for any given solvent packing fraction $\eta = n\pi\sigma^3/6$. n is the bulk number density and σ the hard-sphere diameter. The true difficulty lies in obtaining a reliable value for the packing fraction, η, in a real molecular liquid. Reference 1 gave a technique for estimating the packing fraction from diffusion constant information. The results presented below show that this method overestimates the packing fraction in the liquids studied. This issue will be taken up again in section V. Radial distribution functions in this report, like those in ref 1, were calculated from solutions to the Percus−Yevick equation,[52−56] using an algorithm given by Smith and Henderson,[57] and modified by a Verlet−Weis correction.[58]

The second result from ref 1 is that the distance-dependent diffusion constant can be modeled by a form suggested by Northrup and Hynes, based on work by Deutch *et al*:[41,42,59]

$$D(R) = D\left[1 - \frac{1}{2}\exp\left(\frac{R_m - R}{R_m}\right)\right] \qquad (11)$$

where D is the bulk Fick diffusion constant and R_m the donor−acceptor contact distance. For the neutral rubrene and duroquinone molecules, the Fick diffusion constants were calculated from the Spernol−Wirtz equation.[60] The Spernol−Wirtz equation is a perturbation on the Stokes−Einstein result and has been shown to be highly reliable for neutral molecules diffusing in organic solvents.[60−63] However, much less reliable results are expected for the rubrene and duroquinone ions. The diffusion constant for ions is expected to be significantly slower than for the corresponding neutral parent molecule.[62,64,65] In general, though, ion diffusion rates have been found to agree reasonably well with the predictions of the Stokes−Einstein equation, while neutral species tend to have diffusion constants consistent with Spernol−Wirtz predictions.[60,61,64] Thus, diffusion constants were calculated using

$$D = \frac{kT}{6\pi\eta r f_{sw}}$$

with $f_{sw} = 1$ for the ionic species. For the neutral rubrene and duroquinone molecules, f_{sw} was calculated by the method of Spernol and Wirtz.[60,61] The solvent viscosities, η, were measured using an Ubbelohde viscometer, and the results agreed well with values reported in the literature.[45]

The rubrene and duroquinone ions were assumed to be the same size as the neutrals, and the radii ($r = 4.5$ Å for rubrene and $r = 3.4$ Å for duroquinone) were calculated from crystallographic data.[1,66,67] The procedure for calculating the donor and acceptor radii was described in ref 1 and involves determining the molecular volume from the crystal structures and then reducing this volume by 74% to account for the close packing of hard spheres. This volume can then be used to determine an effective hard-sphere radius.[1] This procedure, when used to predict effective hard-sphere radii for molecular solvents, tends to overestimate the radii by 10−15%,[68] as can be verified by comparison to neutron scattering data, *e.g.* for benzene or naphthalene.[69] For this reason, the radii for rubrene and duroquinone were each reduced an additional 10%.

TABLE 1: Physical Parameters Used in $\langle P_{ex}(t)\rangle$ and $\langle P_{ct}(t)\rangle$ Calculations for the Solvents Dibutyl Phthalate (DBP) and Diethyl Sebacate (DES)[a]

	D_n (Å²/ns)	D_i (Å²/ns)	ϵ_{op}	ϵ_s	$\Delta\xi$ (eV)	τ (ns)	τ_L (ps)
DBP	13.2	6.3	2.2	6.4	1.85	15.5	512
DES	41.5	20.7	2.07	4.7	2.1	15.1	242

[a] D_n and D_i are the (bulk) mutual diffusion coefficients of rubrene and duroquinone in their neutral and ionic states, respectively. ϵ_{op} and ϵ_s are the optical and static dielectric constants, while $\Delta\xi$ is the redox potential difference used in the Rehm−Weller equation (eq 8). τ is the rubrene fluorescence lifetime, and τ_L is the longitudinal relaxation time of the solvent.

Because the donor and acceptor are treated as hard spheres in the model of electron transfer presented here, no angular dependence to the electron transfer rate is included in the analysis. Electron transfer rates are expected to depend on orientation, although the form of this dependence is not well-known. For intermolecular electron transfer, calculation of the observables involves ensemble averaging over all acceptor distances. Rigorously, an angular average should also be included. However, in an earlier publication from this group,[70] a representative calculation was presented that showed that the angular dependence often makes an insignificant contribution to the ensemble-averaged observable. This occurs not because the angular dependence of the transfer rate is small, but because the average over distances and angles results in an ensemble-averaged observable insensitive to orientational contributions.

Solutions to eqs 2 and 7 were obtained using a Crank−Nicholson algorithm following the partial differencing scheme developed by Agmon *et al*.[71−73] All computation was performed on IBM RS6000 workstations. Best fits were determined by a downhill simplex algorithm by minimization of χ^2 values.[73,74] For both the forward and back transfer fits, all acceptor concentrations in a given solvent were fit simultaneously, so that the χ^2 value consisted of the sum of contributions from all the relevant concentrations. For the forward transfer fits, the fluorescence yield data were also included in the χ^2 determination. Table 1 summarizes the physical parameters used in the calculations. See ref 1 for additional details.

V. Results

TCSPC data for rubrene and duroquinone in dibutyl phthalate and diethyl sebacate were presented and analyzed in ref 1 using a detailed theory of electron transfer which included solvent structure and hydrodynamic effects. A Marcus form of the rate constant (eq 9) was used. As discussed in ref 1, accurate determination of the rate parameters requires a good estimate of the solvent packing fraction for calculation of the radial distribution function. For dibutyl phthalate, a packing fraction of 54% was used, and unique forward transfer parameters were obtained: $J_{0f} = 3.1$ cm^{-1} and $\beta_f = 0.6$ Å^{-1}. (The fits to the diethyl sebacate data were not unique.)

The forward transfer parameters, once known from the TCSPC data, serve as inputs into the back transfer calculations. The pump−probe data thus provides a check on the accuracy of the forward transfer fits, since the geminate recombination dynamics depend on the initial distribution of ions formed by forward transfer. More specifically, the back transfer decays cannot be faster than the derivative of the excited state decay. The fastest pump−probe data would occur when the back transfer rate $k_b(R) \rightarrow \infty$. Under this condition, it can be shown

$$\lim_{k_b(R)\to\infty} \langle P_{ct}(t)\rangle \propto -\frac{\partial\langle P_{ex}(t)\rangle}{\partial t}$$

This reflects the fact that, although the ions may disappear immediately upon being formed, new ions are always being created at the rate of loss of excited-state population. Figure 2, curve A, shows the experimental ion population from the pump−probe data for a representative concentration plotted along with the derivative of the $\langle P_{ex}(t)\rangle$ for that concentration, curve B. Clearly, the forward transfer parameters reported in ref 1 are not sufficiently fast to account for the pump−probe data. The new experimental ion population data force reevaluation of the forward transfer dynamics.

i. Forward Transfer Dynamics. As stated in ref 1, the forward parameters depend critically on accurate knowledge of the radial distribution function. Although a hard-sphere model of the solvent was shown to be sufficiently accurate for electron transfer calculations,[1] determination of an effective hard-sphere packing fraction remains a difficult problem for real molecular liquids. Reference 1 provided a method for calculating the packing fraction based on a self-consistent solution of modified Chapman−Enskog theory[75−82] and the Spernol−Wirtz equation. However, for the large molecular solvents, dibutyl phthalate and diethyl sebacate, this led to packing fractions greater than 50%. These numbers are larger than would be expected on the basis of molecular dynamics results, which predict a hard-sphere freezing transition at 49% packing fraction.[56,58,68,83,84] In ref 1 packing fractions of 54 and 53% for dibutyl phthalate and diethyl sebacate, respectively, were justified on the basis of diffusion constant information; however, in light of the new pump−probe data and the molecular dynamics simulations, it is clear that these original packing fractions were too high.

Figures 3 and 4 show the TCSPC data (excited-state decays) for dibutyl phthalate and diethyl sebacate, along with fluorescence yield data obtained in this study. The yield data, as discussed in section IV, serve to solidify the fits from the time-resolved data as well as to distinguish between parameter sets with different short time dynamics. The parameters obtained in ref 1 do not fit the new fluorescence yield data. This confirms the analysis based on the derivative of $\langle P_{ex}(t)\rangle$ that shows the previously reported forward parameters are not correct. The theoretical fits shown in Figures 3 and 4 were calculated from eqs 1 and 10, using a packing fraction of 45% for both solvents rather than the larger values used in ref 1. A packing fraction of 45% was chosen because it is consistent with molecular dynamics results, which predict values between 43 and 48% for dense, room-temperature liquids.[56,58,68,83,84] As can be seen from Figures 3 and 4, excellent fits to the TCSPC and fluorescence yield data are obtained for both dibutyl phthalate and diethyl sebacate. Inclusion of the fluorescence yield information permits a unique fit for the diethyl sebacate data as well as for the dibutyl phthalate data. Furthermore, with a packing fraction of 45%, the forward transfer parameters give $\langle P_{ex}(t)\rangle$ curves with derivatives consistent with the pump−probe data. (See curve C in Figure 2.) By studying both forward transfer and geminate recombination on the same systems it was possible to improve understanding of the forward transfer dynamics.

The precise values of the forward transfer parameters will depend on the chosen packing fraction. For a packing fraction of 45% for both of the solvents, the best fits to the forward transfer data are obtained for $J_{0f} = 12 \pm 3$ cm^{-1}, $\beta_f = 1.4 \pm 0.2$ Å^{-1} and $J_{0f} = 12 \pm 3$ cm^{-1}, $\beta_f = 1.0 \pm 0.2$ Å^{-1} for dibutyl phthalate and diethyl sebacate, respectively. Although the error bars are significant, the parameters are consistent with transfer rates determined from intramolecular electron transfer measurements. Use of the detailed theory presented here, with inclusion of solvent structure and hydrodynamic effects, leads to reasonable values of the Marcus parameters for intermolecular electron transfer. More importantly, the detailed theory provides extremely good fits to the TCSPC and fluorescence yield data in both solvents. In particular, attempts to fit the forward transfer data by assuming reaction only at contact give extremely poor agreement for both solvents. Additionally, even if the full spatial dependence of the problem is included but solvent structure and hydrodynamic effects are ignored, it is impossible to simultaneously fit the TCSPC and fluorescence yield data in either solvent. The best obtainable fits are vastly inferior to those shown in Figures 3 and 4. The success of the detailed

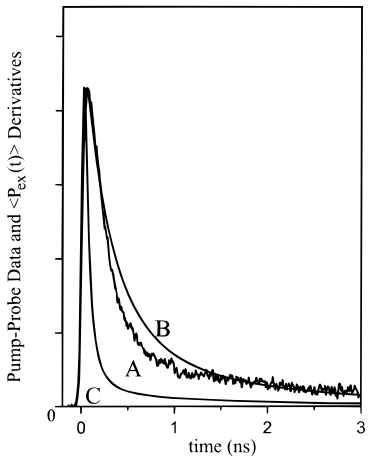

Figure 2. Pump−probe ion population for a rubrene/0.32 M duroquinone sample in dibutyl phthalate (curve A). Curve B is the derivative of the $\langle P_{ex}(t)\rangle$ curve for this concentration, calculated using the forward transfer parameters reported in ref 1 obtained with a solvent packing fraction of 54%. Theory requires that curve B be everywhere faster than curve A, or the forward transfer parameters are not physically possible. Using a better value of the packing fraction, 45%, gives different values for the forward transfer parameters and a $\langle P_{ex}(t)\rangle$ derivative (curve C) that is physically permissible; see text.

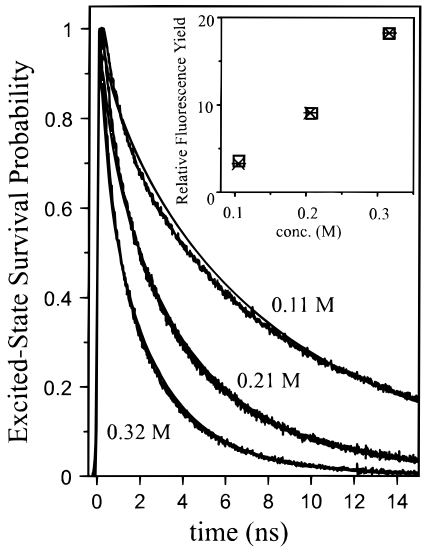

Figure 3. TCSPC and fluorescence yield data for rubrene with three representative concentrations of duroquinone in dibutyl phthalate along with $\langle P_{ex}(t)\rangle$ fits. Forward transfer parameters of $J_{0f} = 11.9$ cm^{-1}, $\beta_f = 1.4$ Å^{-1} give very good agreement for a solvent packing fraction of 45%. In the inset, the squares are the experimental yield results, while the crosses are the calculated values from eq 10. Since donor fluorescence lifetime can be removed from forward transfer by simple multiplication, forward data are shown without lifetime contributions for clarity.

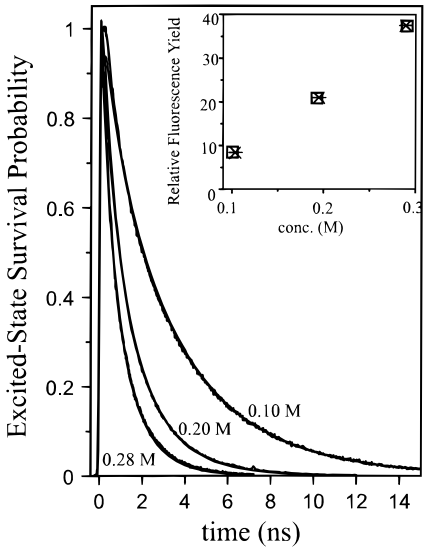

Figure 4. TCSPC and fluorescence yield data for rubrene with three representative duroquinone concentrations in diethyl sebacate along with $\langle P_{ex}(t)\rangle$ fits. The forward transfer fits were calculated with $J_{0f} = 10.8$ cm^{-1}, $\beta_f = 0.96$ Å^{-1} and give very good agreement for a solvent packing fraction of 45%. In the inset, the squares are the experimental yield results, while the crosses are the calculated values from eq 10.

theory presented here is that it is capable of describing experimental data using a physically reasonable model of the molecular liquids. The theory can thus be used to address certain fundamental questions such as how the dynamics depend on diffusion constants, solvent packing fractions, or the donor and acceptor radii.

One source of uncertainty in the reported forward transfer parameters is the solvent packing fraction. Packing fractions from 43 to 48% are consistent with molecular dynamics simulations, and all values in this range give good fits to the forward transfer data and derivatives consistent with the pump−probe data. For a packing fraction of 43% in both solvents, the Marcus parameters that give the best fit to the forward transfer data are $J_{0f} = 12 \pm 3$ cm^{-1}, $\beta_f = 1.5 \pm 0.2$ Å^{-1} and $J_{0f} = 14 \pm 3$ cm^{-1}, $\beta_f = 1.2 \pm 0.2$ Å^{-1} for dibutyl phthalate and diethyl sebacate, respectively. These parameters become $J_{0f} = 9 \pm 2$ cm^{-1}, $\beta_f = 1.2 \pm 0.2$ Å^{-1} (dibutyl phthalate) and $J_{0f} = 11 \pm 2$ cm^{-1}, $\beta_f = 0.9 \pm 0.2$ Å^{-1} (diethyl sebacate) for the two solvents if a packing fraction of 48% is used. The uncertainty in the radial distribution function could be greatly reduced by using solvents for which neutron scattering data are available[69,85] or by using more sophisticated theoretical methods such as the reference interaction site model (RISM)[86] to calculate $g(R)$. However, even given the uncertainty in packing fraction, the parameters do not vary wildly, and none of the qualitative concepts are changed.

The forward transfer parameters in the two solvents are not highly sensitive to the donor−acceptor contact distance. Although careful effort was made to use accurate values for the rubrene and duroquinone radii (see section IV), an error of 5% is possible, and an error of up to 10% is not beyond the realm of possiblity. Inaccuracy in the donor and acceptor radii has the maximum effect on the forward transfer parameters when the error is in the same direction for both radii (*i.e.* the estimates are consistently too large or too small). The rubrene and duroquinone radii used in the fits were 4.5 Å for rubrene and 3.4 Å for duroquinone. If these estimates are reduced by more than 5% each, the quality of the fits deteriorates sharply. For reductions of less than 5%, the forward parameters remain essentially unchanged. On the other hand, if the radii were in fact 5−10% larger than the values reported here, excellent fits

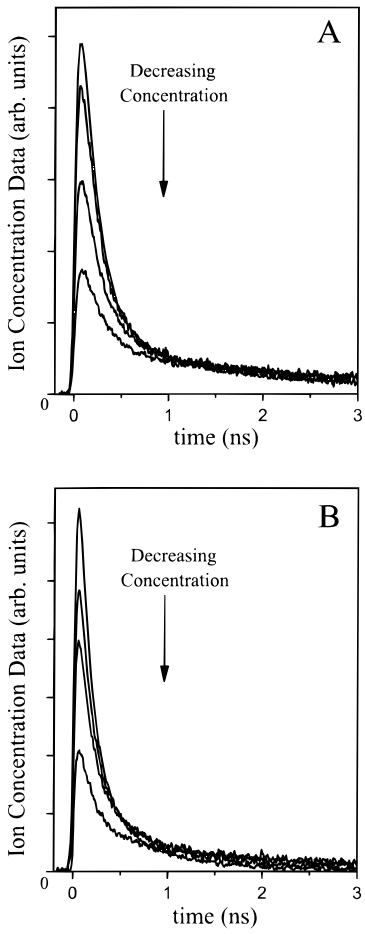

Figure 5. Pump−probe ion concentration data for four concentrations of duroquinone in dibutyl phthalate (A) and diethyl sebacate (B). The figure contains two types of information. First, the time dependence of the ion population is shown, with faster decays corresponding to higher concentrations. Second, within each solvent, the relative magnitudes of the curves reflect the real ratios of ion populations for the different duroquinone concentrations. The duroquinone concentrations are 0.11, 0.21, 0.32, and 0.42 M in dibutyl phthalate and 0.10, 0.20, 0.28, and 0.43 M in diethyl sebacate.

to the TCSPC and fluorescence yield data would still be obtained. The forward transfer parameters then become $J_{0f} = 12 \pm 3$ cm^{-1}, $\beta_f = 1.5 \pm 0.2$ Å^{-1} and $J_{0f} = 9 \pm 2$ cm^{-1}, $\beta_f = 0.9 \pm 0.2$ Å^{-1} for dibutyl phthalate and diethyl sebacate, respectively, for a rubrene radius of 4.7 Å and a duroquinone radius of 3.6 Å (5% increase; 45% packing fraction). For a 10% increase in both radii, the parameters become $J_{0f} = 11 \pm 3$ cm^{-1}, $\beta_f = 1.4 \pm 0.2$ Å^{-1} for dibutyl phthalate and $J_{0f} = 8 \pm 2$ cm^{-1}, $\beta_f = 0.9 \pm 0.2$ Å^{-1} for diethyl sebacate. The β value in particular remains unchanged within the error bars. The detailed theory permits this result to be understood. A change in the donor and acceptor sizes changes the reorganization energy in the Marcus rate equation, the contact distance in all the spatial averaging, the diffusion constant, and the spatial distribution of acceptors about the donor (because of the $4\pi R^2 g(R)$ dependence). Many of these effects work in opposite directions. In particular, as the donor and acceptor become larger, the slowing of the diffusion constant compensates for the increased probability of finding an acceptor near contact due to the $4\pi R^2 g(R)$ distribution.

ii. Geminate Recombination. Once the forward transfer parameters have been determined from the fluorescence yield and TCSPC results, the pump−probe data can be analyzed with eq 4. Figure 5 shows pump−probe data for four acceptor concentrations in each of the two solvents: dibutyl phthalate

(5A) and diethyl sebacate (5B). All curves have had the contribution from rubrene excited-state absorption removed according to the procedure described in Appendix B. Therefore, the plots display the time-dependent ion concentration. Two types of information are contained in the figure. First, the shape of the $\langle P_{ct}(t)\rangle$ decay changes with acceptor concentration. If the curves were scaled to the same magnitude, the rate of decay would be seen to increase with concentration for each solvent. This is consistent with the predictions of eq 4. (Note that although at first glance eq 4 might seem to predict a linear change with concentration, in fact the dependence is more complex, since the $\langle P_{ex}(t)\rangle$ term inside the integral is also concentration dependent.) Rather than presenting the data scaled to the same peak magnitude, Figure 5 instead shows the relative magnitudes of the data in order to illustrate the second type of information inherent in the pump−probe experiments. The procedure given in Appendix B involves correcting all samples for differences in rubrene concentration, so that the difference in height in the data curves is entirely due to the increased number of ions formed at higher acceptor concentrations. Thus, the pump−probe data give not only the time dependence of the back transfer but also the relative amounts of ions formed for different acceptor concentrations. This is a key point. When eq 4 is used to fit the data presented in Figure 5A,B, the theory must not only describe the time dependence of the ion kinetics for all four concentrations but must also correctly predict the relative magnitudes. This is not a trivial requirement.

Examination of Figure 5 shows the qualitative behavior of the ion population. The concentration of ions increases at short time, reaches a maximum, and then decays. The short time behavior is dominated by donors and acceptors that are close at $t = 0$. Little diffusion is required for forward and back transfer to occur. However, there is a long tail to the ion population, which is especially evident in the data taken in dibutyl phthalate (Figure 5A).

Analysis of the pump−probe data with eq 4 requires an expression for the distance-dependent form of the back transfer rate. For the forward transfer rate, the well-known Marcus result (eq 9) was used. For the inverted back transfer, however, eq 9 predicts transfer rates that are orders of magnitude too slow to account for the observed pump−probe data. This breakdown of classical Marcus theory in the inverted regime is expected, since tunneling mechanisms become important for very negative ΔG values. As discussed below, semiclassical forms of the rate constant, such as that suggested by Jortner,[2] provide excellent fits to the pump−probe data. The inclusion of quantum modes in the theory results in more fitting parameters. For this reason, initial analysis of the geminate recombination was performed assuming a simple exponential distance dependence to the back transfer rate. That is,

$$k_b(R) = K \exp[\beta_b(R_m - R)] \qquad (12)$$

Equation 12 is equivalent to assuming that the distance dependence of the reorganization energy can be neglected. This is a reasonable approximation since many more sophisticated descriptions of the electron transfer rate lead to essentially exponential distance dependences for reasonable choices of the quantum parameters. In section VI, the geminate recombination data are analyzed more rigorously using the average mode formalism suggested by Jortner.[2]

Figures 6 and 7 show fits to the pump−probe data using the distance-dependent rate constant given by eq 12. The data curves are identical to those shown in Figure 5A,B, only the results are now displayed in separate panels along with the fits for clarity. The fits were generated using a solvent packing fraction of 45% and the corresponding forward transfer parameters. The adjustable parameters were K and β_b in eq 12. As can be seen, the shapes of the calculated curves at each concentration in both solvents closely reproduce the data. Furthermore, the relative magnitudes of the fits give superb agreement with the experimentally measured relative ion concentrations. These relative magnitudes are predicted by eq 4; the shown fits were not individually scaled to the data sets. The excellent agreement between theory and experiment seen in Figures 6 and 7 cannot be duplicated by simpler theories that ignore solvent structure and hydrodynamic effects. Rather, the statistical mechanical theory presented here with the full inclusion of solvent structure is required. The precise values of the parameters obtained from the fits are discussed in section VI.

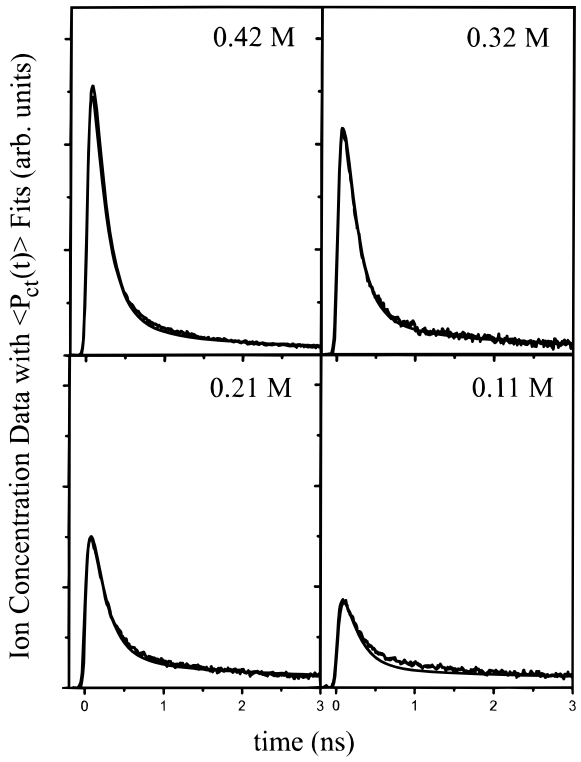

Figure 6. Pump−probe electron transfer data in dibutyl phthalate for four acceptor concentrations showing the time evolution of the ion concentration. The data are the same as those in Figure 5A, only now the curves are shown in separate panels along with the fits so that the quality of the fits can be seen. The fits are essentially indistinguishable from the data. The $\langle P_{ct}(t)\rangle$ fits were calculated using eq 4 with a solvent packing fraction of 45% and the forward transfer parameters given in Figure 3. The only adjustable parameters are K and β_b in eq 12. Superb fits are obtained for both the shape and the relative magnitudes of the curves for $K = 9.5 \pm 1.0$ ns^{-1} and $\beta_b = 1.0 \pm 0.2$ Å^{-1} with a time-dependent dielectric constant (see text). The data were taken with $\lambda_{pump} = 550$ nm and $\lambda_{probe} = 862$ nm.

iii. Ground State Recovery. Since the rubrene/duroquinone system is well modeled by a three-level system (see Figure 1), single-color pump−probe experiments ($\lambda_{pump} = \lambda_{probe} = 550$ nm) on the donor should, in principle, give information about the geminate recombination. If the only absorbing state is the ground state, then the single-color pump−probe signal, $S(t)$, is proportional to the population of rubrene that is not in the ground state.[33] In the simplest case

$$S(t) \propto \langle P_{ex}(t)\rangle + \langle P_{ct}(t)\rangle$$

Since $\langle P_{ex}(t)\rangle$ is known from the TCSPC and fluorescence yield experiments, the radical (ion) survival probability, $\langle P_{ct}(t)\rangle$, could

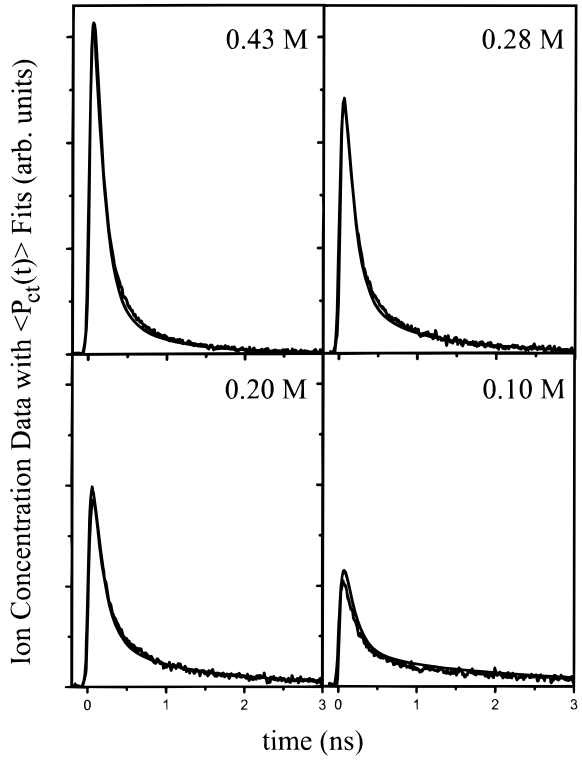

Figure 7. Pump−probe electron transfer data in diethyl sebacate for four acceptor concentrations showing the time evolution of the ion concentration. The data are the same as those in Figure 5B. Fits were calculated using eq 4 with a solvent packing fraction of 45% and the forward transfer parameters given in Figure 4. Excellent fits are obtained for $K = 13.7 \pm 1.0$ ns^{-1} and $\beta_b = 1.3 \pm 0.2$ Å^{-1} with a time-dependent dielectric constant (see text). The data were taken with $\lambda_{pump} = 550$ nm and $\lambda_{probe} = 862$ nm.

be calculated from the ground-state recovery pump−probe data. However, as discussed elsewhere, data analysis of this type is complicated by contributions from stimulated emission and excited-state−excited-state absorption.[33] Furthermore, the short time dynamics are obscured by a coherence artifact in the single-color pump−probe experiments. The chief utility of the ground-state recovery data, then, is to confirm the validity of the three-state model. It is possible that after forward electron transfer, hyperfine interactions convert the radical ions into an overall triplet state.[87,88] If this were to occur, back electron transfer into the rubrene triplet state would become a spin-allowed process, and long-lived rubrene triplets would be generated. This would result in a single color pump−probe signal with a long-time component equal to the triplet lifetime. The single-color pump−probe data show that the rubrene ground state is replenished on the nanosecond time scale, consistent with the ion geminate recovery. This demonstrates the absence of long-lived triplets and supports the three-state model.

VI. Discussion

The theoretical description of intermolecular electron transfer given in eqs 1−7 and used to analyze both the forward and back transfer data includes solvent structure and hydrodynamic effects. Inclusion of these effects is critical for an understanding of intermolecular transfer, and the analysis presented here represents the first attempt to include a realistic description of the solvent in a detailed statistical mechanical treatment of the coupled forward and back transfer processes. Theories that include the full spatial dependence of the electron transfer but neglect the solvent structure cannot provide agreement with the forward transfer data, much less with the pump−probe results.

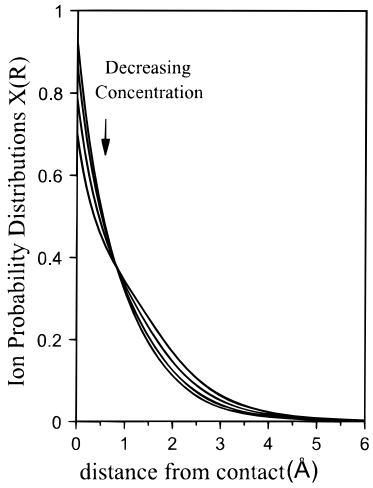

Figure 8. Probability distribution of separations at which ions are created for the donor rubrene and 0.11, 0.21, 0.32, and 0.42 M duroquinone in dibutyl phthalate. As the concentration decreases, increasing fractions of ions are formed at longer distances. In the absence of fluorescence, the probability distribution would integrate to 1.

Inclusion of solvent structure and hydrodynamic effects permits excellent fits to the forward transfer data for both solvents and gives superb agreement with both the shape and magnitude of the pump−probe results.

i. Evidence for Through-Solvent Transfer. The combined forward and back transfer analysis presented here provides evidence that intermolecular electron transfer in liquids occurs through-solvent, rather than only at contact. First, the TCSPC and fluorescence yield data cannot be fit with a model that assumes transfer only at contact. Although forward electron transfer drops off sharply with distance ($\beta \approx 1.4$ for dibutyl phthalate), a detectable fraction of the ions are formed at distances other than contact. This can be seen in Figure 8, which shows the spatial ion probability distribution, $X(R)\,dR$. $X(R)\,dR$ is the probability that an ion is formed between distance R and $R + dR$ from the donor. This distribution is derived in Appendix A and is given by

$$X(R)\,dR = \frac{4\pi CR^2\,dR k_f(R)\int_0^\infty b_{ex}(R,t')\langle P_{ex}(t')\rangle\,dt'}{\int_{R_m}^\infty 4\pi CR^2 k_f(R)\int_0^\infty b_{ex}(R,t')\langle P_{ex}(t')\rangle\,dt'\,dR_0} \quad (13)$$

where $b_{ex}(R,t')$ is the joint probability density given by eq 7. As can be seen from Figure 8, as the acceptor concentration increases, the fraction of transfer at short distances also increases. This occurs because, for higher acceptor concentrations, a larger percentage of donors will have an acceptor nearby at time 0 and will be able to forward transfer immediately after photoexcitation. This result is confirmed by the pump−probe data, which show that decays become increasingly fast as the acceptor concentration increases. The low concentrations display a longer time tail in the pump−probe data due to ions initially created at larger distances which must diffuse in toward the donor before geminate recombination occurs. Figure 8 does not mean that only acceptors that are initially within ~6 Å are involved in electron transfer. Acceptors that are at larger distances at $t = 0$ will diffuse in prior to ion formation.

ii. Solvent Dielectric Response. After forward electron transfer has occurred, the rubrene and duroquinone ions diffuse

in a Coulomb potential as well as in the potential of mean force. (See eq 5.) The magnitude of the Coulomb potential is determined by the value of the dielectric constant. If the static dielectric constant is used in eq 5, the fits to the pump−probe data are the same quality as those displayed in Figures 6 and 7. For dibutyl phthalate, use of the static dielectric constant gives geminate recombination parameters of $K = 12.5 \pm 1.5$ ns^{-1} and $\beta_b = 0.85 \pm 0.15$ Å^{-1}. For diethyl sebacate, good fits to the data are obtained for a broad range of parameters: $K =$ 13.4−17.0 ns^{-1} and $\beta_b = 0.65-1.25$ Å^{-1}.

Although the β values for geminate recombination in dibutyl phthalate and diethyl sebacate are perhaps reasonable within their error bars, the results are based on an inappropriate physical model: namely, that use of the static dielectric constant in eq 5 appropriately describes the Coulomb potential. The static dielectric constant is the relevant value only if the ions exist long enough to experience the full solvent response. As can be seen in Figure 5, the 1/*e* points of the pump−probe curves occur at only a few hundred picoseconds. The mean ion lifetime is expected to be even shorter, since the $\langle P_{ct}(t)\rangle$ curve consists of contributions from many ions, all formed at different times. In fact, as shown in Appendix B, the probability of an ion surviving for time t is given by

$$P(t) = \frac{\int_{R_m}^{\infty} S_{ct}(t|R_0) R_0^{\,2} k_f(R_0) \int_0^{\infty} b_{ex}(R_0,t') \langle P_{ex}(t')\rangle \, dt' \, dR_0}{\int_{R_m}^{\infty} R_0^{\,2} k_f(R_0) \int_0^{\infty} b_{ex}(R_0,t') \langle P_{ex}(t')\rangle \, dt' \, dR_0}$$

where $b_{ex}(R,t)$ satisfies eq 7. The mean ion lifetime, taken as the 1/*e* point of the $P(t)$ curve, is approximately 170 ps in dibutyl phthalate and 120 ps in diethyl sebacate. Thus, it is unlikely that full reorientation of the solvent can occur during the lifetime of the ions; therefore, the static dielectric constant is never reached.

An alternative approach is to take the other extreme and assume that only the electronic response of the solvent can occur on a sufficiently fast time scale, and therefore the dielectric constant in eq 5 should be replaced with the optical one ($\epsilon_{op} \approx$ 2). This is actually not physically realistic, since some molecular motions can occur on time scales of less than 100 ps. However, if as an approximation, the optical dielectric constant is used in eq 5, it is possible to fit the dibutyl phthalate pump−probe data, but the fits are not unique. A very wide range of physically unrealistic parameters can fit the data. Values of $\beta_b = 10-20$ Å^{-1} and $K = 2.6 \times 10^4$ to 4.2×10^6 ns^{-1} are obtained. Notice that these K values correspond to transfer times of a few fractions of a femtosecond to a few tens of femtoseconds. All parameters within this range are unreasonably short-range and give a transfer rate at contact that is unphysical. Furthermore, when the back transfer data taken in the less viscous diethyl sebacate are analyzed using the optical dielectric constant, the theory gives poor fits to the data. The calculated curves, no matter what the choice of parameters, do not have the correct functional form. These results are not surprising, since it seems even more unphysical to consider only the electronic response of the solvent than to use the static dielectric constant throughout the entire ion lifetime. The true dielectric value will evolve in time between these extremes, with a value of the dielectric "constant" changing from ϵ_{op} at the time an ion pair is created to a final value that depends on the lifetime of the particular ion pair under consideration, with a maximum value of ϵ_s.

The effect of a time-dependent dielectric constant can be understood by considering a standard treatment in which the frequency dependence of the dielectric response is that given by Debye:[89]

$$\epsilon(\omega) = \epsilon_{op} + \frac{\epsilon_s - \epsilon_{op}}{1 + i\omega\tau_D} \tag{14}$$

In eq 14, τ_D is the Debye reorientation time:[89]

$$\tau_D = \frac{\eta V}{k_B T} \tag{15}$$

where V is the effective volume occupied by the molecule. Equation 15 assumes stick boundary conditions, which are appropriate for large molecules like dibutyl phthalate and diethyl sebacate, for which interpenetration of the alkyl chains can hinder rotation. For the geminate recombination problem, the solvent response must be known at time t after the creation of an ion. In the simplest case, where the solvent's dielectric response satisfies eq 14, Mozumder has shown that the time-dependent dielectric constant, $\epsilon(t)$, is best described by[90]

$$1/\epsilon(t) = 1/\epsilon_s + (1/\epsilon_{op} - 1/\epsilon_s) \exp(-t/\tau_L) \tag{16}$$

where τ_L is the longitudinal relaxation time, related to the Debye time by

$$\tau_L = \frac{\epsilon_{op}}{\epsilon_s}\tau_D$$

$\epsilon(t)$ should thus be used in place of ϵ_s in eq 5 to obtain the time-dependent potential in the Smoluchowski operator (eq 3). The partial differencing scheme used to solve eq 2 must then be adjusted to allow for diffusion in a time-varying potential.

For the viscous solvent dibutyl phthalate, a reasonable estimate of the Debye relaxation time using eq 15 is $\tau_D = 1.5$ ns. This corresponds to slow reorientation of the entire molecule and is consistent with experimentally measured reorientation times in viscous solvents.[91] Use of $\tau_D = 1.5$ ns ($\tau_L = 512$ ps) in eq 16 gives $\epsilon(t)$ which, when used in eq 5, gives excellent fits to both the magnitude and time dependence of the pump−probe data in dibutyl phthalate. The best fits are displayed in Figure 6 and occur for parameters $K = 9.5 \pm 1.0$ ns^{-1} and $\beta_b = 1.0 \pm 0.2$ Å^{-1}. For diethyl sebacate, reasonable estimates of the molecular volume in combination with eq 15 give a Debye reorientation time (τ_D) of 550 ps. This value is in agreement with experimentally measured reorientation times of long-chain alkyl derivatives. For example, an orientation time of 840 ps has been measured by Rayleigh scattering for 1-hexadecyl bromide.[92] Hexadecyl bromide is about the same size as diethyl sebacate. The reorientation time in diethyl sebacate should then be similar to that of hexadecyl bromide, only reduced by the ratio of the viscosities. Calculations of this type give a Debye reorientation time for diethyl sebacate of 500−600 ps, consistent with the predictions of eq 15. When a value of 550 ps is used for the Debye time of diethyl sebacate ($\tau_L = 242$ ps), excellent fits to the pump probe data are obtained for electron back transfer parameters of $K = 13.7 \pm 1.0$ ns^{-1} and $\beta_b = 1.3 \pm 0.2$ Å^{-1}. These are the fits shown in Figure 7. The fits are now unique; that is, there is no longer a broad range of parameters that can fit the data as was found when the static dielectric constant was used. Similar values of the parameters are obtained for other estimates of the Debye relaxation time within the range 500−600 ps.

The preceding discussion has assumed that the solvent dielectric behavior is characterized by a single orientational mode that accompanies the faster electronic response. However, the response of a solvent to the introduction of a polar or charged

species is expected to occur over several time scales.[12,93−98] A review of experimental information and interpretations is given in ref 93. Short time, partial reorientational contributions to the dielectric constant could then be modeled by a sum of terms like those in eqs 14 and 16. Evaluation of these terms would require specific information about the solvent response. While more sophisticated models of dielectric relaxation are not included in the data analysis presented here, the Debye relaxation model used nonetheless contains the essential features of the solvent's dielectric response for the geminate recombination of ions formed by forward photoinduced electron transfer. It seems clear that neither extreme of the optical or static dielectric constant can provide a realistic description of the Coulomb potential for the short-lived ions. The fits displayed in Figures 6 and 7, using a time-dependent dielectric constant given by eq 16, yield geminate recombination parameters of $K = 9.5 \pm 1.0$ ns^{-1} and $\beta_b = 1.0 \pm 0.2$ Å^{-1} for dibutyl phthalate and $K = 13.7 \pm 1.0$ ns^{-1} and $\beta_b = 1.3 \pm 0.2$ Å^{-1} for diethyl sebacate. Note that inclusion of a time-dependent dielectric constant results in a narrower range of parameters capable of fitting the ion kinetics in diethyl sebacate. In addition, when the Coulomb potential varies in time, the β_b values are similar in the two solvents and are consistent with what is known from studies of intramolecular electron transfer.[99,100]

iii. Quantum Mechanical Extensions to the Rate Constant. A key point to be addressed in the analysis of the geminate recombination (ion survival) kinetics is the validity of eq 12, which assumes a rate constant that varies exponentially with distance. Although a standard Marcus form of the rate constant (eq 9) was used for the forward transfer data, this classical result cannot describe the geminate recombination dynamics. For highly inverted reactions, like the back electron transfer studied here, eq 9 predicts a transfer rate that is orders of magnitude too slow to account for the observed data. This failure of the classical Marcus expression in the inverted regime has been observed by others.[11] When the free energy change for the reaction is sufficiently large, tunneling pathways become dominant, and more rigorous quantum mechanical treatments are needed.[2,11,29,30,50,51]

A convenient treatment, suggested by Jortner,[2] is to assume that the multiple quantum modes can be treated as a single mean mode of frequency ν. The distance-dependent rate constant then becomes[2,30,51]

$$k_b(R) = \frac{2\pi}{\hbar\sqrt{4\pi\lambda_s(R)k_BT}} J_{0b}^2 \sum_{n=0}^{\infty} \frac{e^{-S}S^n}{n!} \times \exp\left(\frac{-(\Delta G_b(R) + \lambda_s(R) + nh\nu)^2}{4\lambda_s(R)k_BT}\right) \exp(-\beta_b(R - R_m)) \quad (17)$$

$$S = \frac{\lambda_v}{h\nu}$$

λ_v is the reorganization energy associated with the mean high-frequency mode, while λ_s is the classical solvent reorganization energy, given approximately by eq 9b. $\Delta G_b(R)$ is the free energy change for the back transfer process. For geminate recombination between the duroquinone anion and the rubrene cation in dibutyl phthalate and diethyl sebacate, the parameters ν, λ_v, J_{0b}, and β_b need to be determined. Given the lack of knowledge of ν and λ_v for the system under study, an actual fit of the data would involve four adjustable parameters. Such a fit would not be particularly meaningful. Therefore, reasonable choices for the mean quantum mode's frequency and reorganization energy were used, *i.e.*, $\nu = 1550$ cm^{-1} and $\lambda_v = 0.4$ eV, leaving J_{0b}, and β_b the two unknowns as before. A mean frequency of 1550 cm^{-1} corresponds to a typical aromatic stretch, while λ_v values between 0.2 and 0.6 eV are reasonable for aromatic molecules such as rubrene and duroquinone.[19,51] For the given choices of ν and λ_v and using eq 17 for the distance dependence of the transfer rate, excellent fits to the pump−probe data were obtained. Using the time-dependent dielectric constant as above, the parameters are $J_{0b} = 16.5 \pm 1.0$ cm^{-1} and $\beta_b = 1.1 \pm 0.2$ Å^{-1} for dibutyl phthalate and $J_{0b} = 33 \pm 1$ cm^{-1} and $\beta_b = 1.3 \pm 0.2$ Å^{-1} for diethyl sebacate. The β_b are the same, within error, as those determined using the exponential distance dependence for the transfer rate. In addition, the J_{0b} values, when combined with the other parameters in eq 17, give essentially the same transfer rate at contact as obtained with the exponential distance-dependent transfer rate. The quantum mechanical theory provides insight into the factors that control the transfer rate. However, in the absence of specific knowledge of ν and λ_v, the simpler exponential distance dependence appears to be able to provide information on the distance dependence of the transfer rate and the rate at contact. Within a range, other choices of ν and λ_v give equally good fits. If λ_v is varied between 0.2 and 0.6 eV for a constant $\nu = 1550$ cm^{-1}, the β_b values change by ± 0.2 Å^{-1}, the error bars reported above.

As a final point, it should be noted that the solvent reorganization energy, λ_s in eq 17, should vary with time due to the solvent's time-dependent dielectric response. Some experimental evidence for a time-dependent reorganization energy has been reported in the literature,[51] and understanding the role of slow solvent reorientation is an area of ongoing research.[10,12,14,15,93,101−106]

VII. Conclusions

The pump−probe experiments presented here, when combined with the TCSPC and fluorescence yield data, provide a complete description of the forward transfer and geminate recombination dynamics for an intermolecular electron transfer system in liquid solvents. Although the problem of electron transfer in liquids is one of continuing interest, few researchers have studied both the forward and back transfer. This work describes the coupled process in a rigorous way, including both the full spatial dependence of the problem and the dramatic influence of solvent structure and hydrodynamic effects. The analysis is limited to some extent by the ability to know precise microscopic details about a real molecular solvent. Most significant is uncertainty in the solvent's radial distribution function and time-dependent dielectric constant. These quantities, however, are in principle experimentally obtainable. Neutron scattering and time-dependent fluorescence shift measurements can provide direct information about $g(R)$ and $\epsilon(t)$, respectively. In the absence of neutron (or X-ray) scattering data, more sophisticated theoretical methods can be used to calculate the radial distribution function. Future work in this laboratory will concentrate on using a reference interaction site model (RISM) to calculate improved distribution functions.[86]

The mild spread in electron transfer rate parameters that arises from uncertainties in microscopic properties of the solute/solvent systems should not obscure the substantial success of the detailed theory. The model of photoinduced forward and back electron transfer makes a serious effort to include all the physically relevant features of the solute/solvent system. It should be stressed that photoinduced forward and back electron transfer dynamics in liquids is an extremely complex problem. Prior

to this work, no theoretical method existed that included both (1) rigorous ensemble-averaging techniques and (2) an incorporation of physically relevant aspects of solvent structure and hydrodynamic effects. The current theory includes solvent structural effects in a detailed theory of electron transfer and thus at last enables certain key questions to be addressed. The extent to which the hydrodynamic effect and the radial distribution function play off against one another, the role of diffusion, and the dependence on solvent radial distribution function can now be studied with theoretical rigor. These types of questions cannot be addressed with simpler theories.

In addition to providing a meaningful framework in which to analyze electron transfer dynamics in liquids, the theory also provides excellent fits to TCSPC and pump−probe data in cases where these data could not be fit with previous models. Furthermore, the rate parameters required to achieve these fits are reasonable and consistent with studies of intramolecular electron transfer. It is remarkable that a two-parameter fit to the pump−probe data can yield the correct shape and relative magnitudes for samples with four different acceptor concentrations.

The description of intermolecular electron transfer in solution remains an area of ongoing research. The work presented here and in refs 1 and 3 is the first to include structural effects in a full statistical mechanical treatment of the coupled forward and back transfer problem. These effects have been demonstrated to be necessary to obtain an understanding of electron transfer dynamics in liquids.

Acknowledgment. We would like to thank Professor Hans C. Andersen, Department of Chemistry, Stanford University, for continuing discussions on the calculation of radial distribution functions. We would also like to thank Professor David Chandler, Department of Chemistry, University of California at Berkeley, and Professor John D. Weeks, University of Maryland, for providing further insights into the calculation of radial distribution functions. We also gratefully acknowledge Professors David Siegmund and Jerry Friedman, Department of Statistics, Stanford University, for their assistance with statistical analysis of χ^2 results in data fitting. This research was supported by the Department of Energy, Office of Basic Energy Sciences (Grant DE-FG03-84ER13251). H.L.T. was supported by a graduate fellowship from the Office of Naval Research.

Appendix A. Derivation of Eq 6

When a potential other than that caused by the solvent's radial distribution function exists between the donor and acceptor prior to forward transfer, eq 4 no longer rigorously describes the ion kinetics. Instead, eq 6 must be used. Equation 6 is the general result for any form of the distance-dependent potential in the forward or back transfer step. The derivation begins by writing equations analogous to eq 2, only for the joint probability density, $d_{ex}(R,t)$, rather than the conditional survival probability $S_{ex}(t|R_0)$. $d_{ex}(R,t)$ is the joint probability density (probability per unit volume) that the donor is still excited and the acceptor is at R at time t for the two-particle problem (one donor and one acceptor). $d_{ex}(R,t)$ satisfies the differential equation with initial condition

$$\frac{\partial}{\partial t}d_{ex}(R,t) = L_R d_{ex}(R,t) - k_f(R)\, d_{ex}(R,t) \qquad \text{(A1)}$$

$$d_{ex}(R,0) = \frac{g(R)}{V} \qquad \text{(A2)}$$

The probability that the donor is still excited at time t and the acceptor is at R is then $d_{ex}(R,t)4\pi R^2\, dR$. In eqs A1-A2, V is the volume of the system, which goes to infinity in the thermodynamic limit, and L_R is the Smoluchowski operator, rather than the adjoint of the Smoluchowski operator, $L^+_{R_0}$.[23,44] That is, in eq A1

$$L_R = \frac{1}{R^2}\frac{\partial}{\partial R}\left[R^2 D(R)\exp(-V(R))\frac{\partial}{\partial R}[\exp(V(R))]\right] \qquad \text{(A3)}$$

For ease in taking the thermodynamic limit later in the derivation, one defines

$$b_{ex}(R,t) = V d_{ex}(R,t)$$

so that $b_{ex}(R,t)$ satisfies eq A1, but with initial condition

$$b_{ex}(R,0) = g(R) \qquad \text{(A4)}$$

In deriving $\langle P_{ct}(t)\rangle$ for the N acceptor problem, one begins by writing[39]

$$\frac{\partial}{\partial t}P^i_{ct}(R_1...R_N,t|R_{01}...R_{0N}) = \sum_{j=1}^{N} L_{R_j} P^i_{ct}(R_1...R_N,t|R_{01}...R_{0N}) - k_b(R_i)P^i_{ct}(R_1...R_N,t|R_{01}...R_{0N}) + k_f(R_i)P_{ex}(R_1...R_N,t|R_{01}...R_{0N}) \qquad \text{(A5)}$$

where $P^i_{ct}(R_1...R_N,t|R_{01}...R_{0N})$ is a probability density; given that the acceptors were at $R_{01}...R_{0N}$ at time 0, $P^i_{ct}(R_1...R_N,t|R_{01}...R_{0N})$ is the probability per unit volume that at time t the donor is an ion and the N acceptors are at $R_1...R_N$, with the ith acceptor possessing the electron. Similarly, $P_{ex}(R_1...R_N,t|R_{01}...R_{0N})$ is the probability density that the donor is excited at time t with the acceptors at $R_1...R_N$. Calculation of $\langle P_{ct}(t)\rangle$ involves taking the ensemble average of A5. The ensemble average is formally defined:

$$\langle P_{ct}(t)\rangle = N\langle P^i_{ct}(t)\rangle \equiv N\int_{R_1}...\int_{R_N}\int_{R_{01}}... \int_{R_{0N}} P^i_{ct}(R_1...R_N,t|R_{01}...R_{0N})4\pi {R_1}^2...4\pi {R_N}^2\, dR_1...dR_N \times \frac{4\pi {R_{01}}^2 g(R_{01})}{V}...\frac{4\pi {R_{0N}}^2 g(R_{0N})}{V}\, dR_{01}...dR_{0N} \qquad \text{(A6)}$$

where the $4\pi R_i^2\, dR_i$ terms convert from a probability density to a probability and the $4\pi R_{0i}^2 g(R_{0i})/V$ terms give the likelihood of the acceptors being located at $R_{01}...R_{0N}$ at time 0. The factor of N is required since any of the N acceptors could receive the electron.

As has been shown previously, calculation of $\langle P_{ct}(t)\rangle$ involves ensemble averaging eq A5 over all R_j and R_{0j} ($j \neq i$) before solving the differential equation.[39] That is

$$\frac{\partial}{\partial t}P^i_{ct}(R_i,t|R_{0i}) = L_{R_i}P^i_{ct}(R_i,t|R_{0i}) - k_b(R_i)\, P^i_{ct}(R_i,t|R_{0i}) + k_f(R_i)\, G_{ex}(R_i,t|R_{0i})\langle P_{ex}(t)\rangle \qquad \text{(A7)}$$

where $P^i_{ct}(R_i,t|R_{0i})$ is $P^i_{ct}(R_1...R_N,t|R_{01}...R_{0N})$ averaged over all R_j and R_{0j} for $j \neq i$. (Average defined as in eq A6.) $G_{ex}(R_i,t|R_{0i})$ is the Green's function for the two-body problem; that is, for one donor and one acceptor, $G_{ex}(R_i,t|R_{0i})$ is the probability density that at time t the donor is excited and the acceptor is at R_i, given that the acceptor started at R_{0i} at time 0. $G_{ex}(R_i,t|R_{0i})$ satisfies a differential equation similar to eq A1. Averaging eq A7 over R_{0i} and defining

$$P^i_{ct}(R_i,t) \equiv \int_{R_{0i}} P^i_{ct}(R_i,t|R_{0i})\frac{4\pi {R_{0i}}^2 g(R_{0i})}{V}\, dR_{0i}$$

one obtains

$$\frac{\partial}{\partial t}P^{i}_{ct}(R_i,t) = L_{R_i}P^{i}_{ct}(R_i,t) - k_b(R_i)\,P^{i}_{ct}(R_i,t) + k_f(R_i)\langle P_{ex}(t)\rangle \int_{R_{0i}} G_{ex}(R_i,t|R_{0i})\,\frac{4\pi {R_{0i}}^2 g(R_{0i})}{V}\,dR_{0i} \quad \text{(A8)}$$

The integral in the third term is simply the joint probability density $d_{ex}(R_i,t)$. Equation A8 thus has a solution[39]

$$P^{i}_{ct}(R_i,t) = \frac{1}{V}\int_0^t \int_{R_m}^{\infty} G_{ct}(R_i,t-t'|R_0)\,k_f(R_0)\,b_{ex}(R_0,t') \times \langle P_{ex}(t')\rangle 4\pi {R_0}^2\,dR_0\,dt' \quad \text{(A9)}$$

where $G_{ct}(R_i,t|R_{0i})$ is the Green's function for the reactive state; that is, for one donor and one acceptor, given that at time 0 the acceptor is an anion at R_{0i}, $G_{ct}(R_i,t|R_{0i})$ is the probability density that at time t the acceptor is at distance R_i from the donor and back transfer has not yet occurred.

Calculation of $\langle P_{ct}(t)\rangle$ now involves performing the final integral over R_i, *i.e.*

$$\langle P_{ct}(t)\rangle = N\langle P^{i}_{ct}(t)\rangle = N\int_{R_i} P^{i}_{ct}(R_i,t)4\pi {R_i}^2\,dR_i$$

$$= \frac{N}{V}\int_0^t \int_{R_m}^{\infty} [\int_{R_i} G_{ct}(R_i,t-t'|R_0)4\pi {R_i}^2\,dR_i] \times k_f(R_0)\,b_{ex}(R_0,t')\langle P_{ex}(t')\rangle 4\pi {R_0}^2\,dR_0\,dt' \quad \text{(A10)}$$

The bracketed term in eq A10 is the survival probability $S_{ct}(t|R_{0i})$, or the probability that the donor and acceptor radicals exist at time t given that the acceptor radical was at R_{0i} at time 0. $S_{ct}(t|R_{0i})$ is a conditional probability, rather than a joint probability density like $b_{ex}(R,t)$. That is, $S_{ct}(t|R_{0i})$ involves averaging the Green's function over all ending positions, while $b_{ex}(R,t)$ involves integrating the Green's function over all starting positions. Hence, $S_{ct}(t|R_{0i})$ satisfies eq 2 of the main text (with the adjoint Smoluchowski operator) and initial condition $S_{ct}(0|R_{0i}) = 1.0$, while $b_{ex}(R,t)$ satisfies eq A1 involving the nonadjoint operator and an initial condition $b_{ex}(R,0) = g(R)$.

In the thermodynamic limit, $N/V \rightarrow C$ (the concentration) and

$$\langle P_{ct}(t)\rangle = 4\pi C\int_{R_m}^{\infty}\int_0^t S_{ct}(t-t'|R_0)\,k_f(R_0)\,b_{ex}(R_0,t')\langle P_{ex}(t')\rangle {R_0}^2\,dR_0\,dt' \quad \text{(A11)}$$

which is eq 6 of the main text.

Equation A9 can also be used to calculate the distribution of ions formed by forward transfer. $X(R)\,dR$ is the probability that the ion pair was created at the separation distance between R and $R + dR$. If both the back transfer rate and the ion diffusion constant are set equal to zero, then the ions are "frozen" immediately upon creation. $X(R)\,dR$ is then obtained by multiplying eq A9 by $4\pi NR^2$ and taking the infinite-time limit:

$$X(R)\,dR = \frac{4\pi CR^2\,dR k_f(R)\int_0^{\infty} b_{ex}(R,t')\langle P_{ex}(t')\rangle\,dt'}{\int_{R_m}^{\infty} 4\pi CR^2 k_f(R)\int_0^{\infty} b_{ex}(R,t')\langle P_{ex}(t')\rangle\,dt'\,dR} \quad \text{(A12)}$$

The denominator in eq A12 normalizes the probability distribution.

Once the distribution of ions formed by forward transfer is known from eq A12, the probability of an ion surviving time t, $P(t)$, can then be calculated from[33]

$$P(t) = \int_{R_m}^{\infty} S_{ct}(t|R_0)\,X(R_0)\,dR_0 \quad \text{(A13)}$$

Appendix B. Removing Excited-State−Excited-State Absorption from the Pump−Probe Signal

For the two-color pump−probe experiments, although the probe beam was tuned over more than 100 nm (840−980 nm), no region could be found where the signal arose entirely from the rubrene cation. At all probe wavelengths, significant contribution to the signal came from a rubrene excited-state−excited-state absorption. This appendix describes the procedure used to remove the excited-state contribution to the pump−probe signal without needing to know the absorption coefficient for either the rubrene cation or the rubrene excited state.

For each solvent, five samples of reasonably similar rubrene concentration were prepared: one pure rubrene sample plus samples with rubrene and four different duroquinone concentrations. TCSPC and fluorescence yield experiments were then performed. Analysis of the forward transfer data gave $\langle P_{ex}(t)\rangle$ for each sample, so that the kinetics of the excited-state decay were known prior to performing the pump−probe experiments. Pump−probe signals were then recorded for each of the five samples.

Immediately after recording the pump−probe scans, a series of additional measurements were made. First, for each sample, several points in the decay were chosen (usually 200, 500, and 1000 ps). The intensities of the signals for all the samples were then measured at each time in rapid succession under the same laser power conditions. Multiple measurements were made to minimize error. Second, the rubrene absorption in all the samples was determined in the laboratory, directly with the laser excitation beam. This was essential to ensure that the results correctly reflected the bandwidth characteristics of the excitation beam to give the true absorption by the samples at the time of the experiment. Subsequent measurement of rubrene absorption by a UV−vis spectrometer was found not to be sufficient, since such equipment does not reproduce the exact color and bandwidth of the laser excitation beam. The absorption measurements, like the intensity readings at the selected time points, were performed immediately following the pump−probe experiment.

To remove the excited-state contribution to the pump−probe signal, the pump−probe results must first be scaled to correct for differences in experimental conditions and in rubrene concentration. Since all samples were scanned on the same day, the only difference in the experimental conditions came from a very slow loss of pump power. (All other conditions that could have affected the pump−probe signal were monitored and remained constant.) The intensity loss was very much slower than the data averaging rate. Thus, there was no error in the pump−probe shapes, only in the magnitude of the signals. The full data scans were scaled to provide agreement with the measured ratios recorded at the selected time points. The signals were then scaled to remove differences due to rubrene concentration. To scale a sample, S_1, with a rubrene absorption A_1 to that of a sample, S_2, with absorption A_2, division is by the factor

$$\frac{S_1}{S_2} = \frac{1-10^{-A_1}}{1-10^{-A_2}}$$

The scaling procedure described above corrects the pump−probe results to those that would be obtained from five samples with identical rubrene concentrations measured with the same laser power. The excited-state contribution can then be removed

using the known $\langle P_{ex}(t)\rangle$ results from the forward transfer experiments. The magnitudes of the $\langle P_{ex}(t)\rangle$ curves for the five samples are not arbitrary. Since $\langle P_{ex}(t)\rangle$ is a probability, the value of 1.0 (unit probability) means that all the excited states created by the pump pulse are still excited. For the corrected pump−probe results, the number of excited states created by the pump beam is the same for all five samples. The relative contribution of the excited-state−excited-state decay to the pump−probe signals can be obtained by convolving the theoretical $\langle P_{ex}(t)\rangle$ curves with the pump−probe instrument response. The resulting convolved $\langle P_{ex}(t)\rangle$ curves will be of different magnitudes, but with ratios corresponding to real time-dependent differences in the number of excited states. Now, since one of the samples contains pure rubrene with no acceptors, the pump−probe signal for that sample is simply the rubrene excited-state decay, *i.e.*, the appropriately convolved $\langle P_{ex}(t)\rangle$, which in this case is just a convolved single-exponential decay at the fluorescence lifetime. Some scaling factor, *S*, then exists that will scale the theoretical (convolved) $\langle P_{ex}(t)\rangle$ curve to the pure rubrene pump−probe signal, so that subtraction of the two curves gives a value of 0 everywhere, *i.e.*, no contribution from the ions since there are no acceptors. Since all five samples have been corrected to the same donor concentration, then the same number of rubrene molecules are excited by the pump beam, *and the scaling factor S is the appropriate scaling factor for all the samples*. If the calculated $\langle P_{ex}(t)\rangle$ curves, including convolutions, are now scaled by *S*, this gives exactly the excited-state contribution to the pump−probe signal and can be directly subtracted from the data. The remaining signal must be due to the ions.

References and Notes

(1) Swallen, S. F.; Weidemaier, K.; Tavernier, H. L.; Fayer, M. D. *J. Phys. Chem.* **1996**, *100*, 8106.
(2) Jortner, J. *J. Chem. Phys.* **1976**, *64*, 4860.
(3) Swallen, S. F.; Weidemaier, K.; Fayer, M. D. *J. Chem. Phys.* **1996**, *104*, 2976.
(4) Marcus, R. A. *J. Chem. Phys.* **1956**, *24*, 966.
(5) Marcus, R. A. *Annu. Rev. Phys. Chem.* **1964**, *15*, 155.
(6) Hush, N. S. *Trans. Faraday Soc.* **1961**, *57*, 557.
(7) Therien, M. J.; Selman, M.; Gray, H. B.; Chang, I.-J.; Winkler, J. R. *J. Am. Chem. Soc.* **1990**, *112*, 2420.
(8) Langen, R.; Chang, I.-J.; Germanas, J. P.; Richards, J. H.; Winkler, J. H.; Gray, H. B. *Science* **1995**, *268*, 1733.
(9) Franzen, S.; Boxer, S. G. *J. Phys. Chem.* **1993**, *97*, 6304.
(10) Wiederrecht, G. P.; Watanabe, S.; Wasielewski, M. R. *Chem. Phys.* **1993**, *176*, 601.
(11) Walker, G. C.; Akesson, E.; Johnson, A. E.; Levinger, N. E.; Barbara, P. F. *J. Phys. Chem.* **1992**, *96*, 3728.
(12) Weaver, M. J. *Chem. Rev.* **1992**, *92*, 463.
(13) Barbara, P. F.; Walker, G. C.; Smith, T. P. *Science* **1992**, *256*, 975.
(14) Simon, J. D.; Su, S. *J. Chem. Phys.* **1987**, *87*, 7016.
(15) Bagchi, B. *Annu. Rev. Phys. Chem.* **1989**, *40*, 115.
(16) Miller, R. J. D.; McLendon, G. L.; Nozik, A. J.; Schmickler, W.; Willig, F. *Surface Electron Transfer Processes*; VCH: New York, 1995.
(17) Miller, J. R.; Calcaterra, L. T.; Closs, G. L. *J. Am. Chem. Soc.* **1984**, *106*, 3047.
(18) Cortes, J.; Heitele, H.; Jortner, J. *J. Phys. Chem.* **1994**, *98*, 2527.
(19) Asahi, T.; Ohkohchi, M.; Matsusaka, R.; Mataga, N.; Zhang, R. P.; Osuka, A.; Maruyama, K. *J. Am. Chem. Soc.* **1993**, *115*, 5665.
(20) Hormann, A.; Jarzeba, W.; Barbara, P. F. *J. Phys. Chem.* **1995**, *99*, 2006.
(21) Penfield, K. W.; Miller, J. R.; Paddon-Row, M. N.; Cotsaris, E.; Oliver, A. M.; Hush, N. S. *J. Am. Chem. Soc.* **1987**, *109*, 5061.
(22) Rice, S. A. *Diffusion-Limited Reactions*; Elsevier: Amsterdam, 1985.
(23) Smoluchowski, M. V. *Z. Phys. Chem. (Leipzig)* **1917**, *92*, 129.
(24) Collins, F. C.; Kimball, G. E. *J. Colloid Sci.* **1949**, *4*, 425.
(25) Shannon, C. F.; Eads, D. D. *J. Chem. Phys.* **1995**, *103*, 5208.
(26) Murata, S.; Nishimura, M.; Matsuzaki, S. Y.; Tachiya, M. *Chem. Phys. Let.* **1994**, *219*, 200.
(27) Kakitani, T.; Matsuda, N.; Yoshimori, A.; Mataga, N. *Prog. React. Kinet.* **1995**, *20*, 347.
(28) Levich, V. G. *Adv. Electrochem. Electrochem. Eng.* **1966**, *4*, 249.
(29) Ulstrup, J.; Jortner, J. *J. Chem. Phys.* **1975**, *63*, 4358.
(30) Marcus, R. A.; Sutin, N. *Biochim. Biophys. Acta* **1985**, *811*, 265.
(31) Tachiya, M. *Radiat. Phys. Chem.* **1983**, *21*, 167.
(32) Murata, S.; Matsuzaki, S. Y.; Tachiya, M. *J. Phys. Chem.* **1995**, *99*, 5354.
(33) Song, L.; Swallen, S. F.; Dorfman, R. C.; Weidemaier, K.; Fayer, M. D. *J. Phys. Chem.* **1993**, *97*, 1374.
(34) Fayer, M. D.; Song, L.; Swallen, S. F.; Dorfman, R. C.; Weidemaier, K. In *Ultrafast Dynamics of Chemical Systems*; Simon, J. D., Ed.; Kluwer Academic Publishers: Amsterdam, 1994; pp 37−80.
(35) (a) Dorfman, R. C.; Fayer, M. D. *J. Chem. Phys*. **1992**, *96* 7410. (b) Burshtein, A. I. *Chem. Phys. Lett*. **1992**, *194*, 247. References 35a and 35b give the original derivation of the exact statistical mechanical theory of geminate recombination in simple (featureless) solvents. These references were incorrectly cited in refs 1 and 3.
(36) Dorfman, R. C.; Tachiya, M.; Fayer, M. D. *Chem. Phys. Lett.* **1991**, *179*, 152.
(37) Burshtein, A. I.; Zharikov, A. A.; Shokhirev, N. V.; Spirina, O. B.; Krissinel, E. B. *J. Chem. Phys.* **1991**, *95*, 8013.
(38) Burshtein, A. I. *J. Chem. Phys.* **1995**, *103*, 7927.
(39) Dorfman, R. C.; Fayer, M. D. *J. Chem. Phys.* **1992**, *96*, 7410.
(40) Burshtein, A. I. *Chem. Phys. Lett.* **1992**, *194*, 247.
(41) Wolynes, P. G.; Deutch, J. M. *J. Chem. Phys.* **1976**, *65*, 450.
(42) Northrup, S. H.; Hynes, J. T. *J. Chem. Phys.* **1979**, *71*, 871.
(43) Swallen, S. F.; Fayer, M. D. *J. Phys. Chem.* **1995**, *103*, 8864.
(44) Agmon, N.; Szabo, A. *J. Chem. Phys.* **1990**, *92*, 5270.
(45) Riddick, J. A.; Bunger, W. B.; Sakano, T. K. *Organic Solvents: Physical Properties and Methods of Purification*, 4th ed.; John Wiley & Sons: New York, 1986.
(46) Rehm, D.; Weller, A. *Isr. J. Chem.* **1970**, *8*, 259.
(47) Chanon, M.; Hawley, M. D.; Fox, M. A. In *Photoinduced Electron Transfer. Part A*; Fox, M. A., Chanon, M., Eds.; Elsevier: New York, 1988; pp 1−60.
(48) Bolton, J. R.; Archer, M. D. . In *Electron Transfer in Inorganic, Organic, and Biological Systems*; Bolton, J. R., Mataga, N., McLendon, G., Eds.; The American Chemical Society: Washington, DC, 1991; p 7.
(49) Shida, T. *Electronic Absorption Spectra of Radical Ions*; Elsevier: Amsterdam, 1988.
(50) Jortner, J.; Bixon, M. *J. Chem. Phys.* **1988**, *88*, 167.
(51) Miller, J. R.; Beitz, J. V.; Huddleston, R. K. *J. Am. Chem. Soc.* **1984**, *106*, 5057.
(52) Percus, J. K.; Yevick, G. Y. *Phys. Rev.* **1958**, *120*, 1.
(53) Percus, J. K. *Phys. Rev. Lett.* **1962**, *8*, 462.
(54) Thiele, E. *J. Chem. Phys.* **1963**, *39*, 474.
(55) Wertheim, M. S. *Phys. Rev. Lett.* **1963**, *10*, 321.
(56) Throop, G. J.; Bearman, R. J. *J. Chem. Phys.* **1965**, *42*, 2408.
(57) Smith, W. R.; Henderson, D. *Mol. Phys.* **1970**, *19*, 411.
(58) Verlet, L.; Weis, J. J. *Phys. Rev. A* **1972**, *5*, 939.
(59) Deutch, J. M.; Felderhof, B. U. *J. Chem. Phys.* **1973**, *59*, 1669.
(60) Spernol, A.; Wirtz, K. *Z. Naturforsch. Teil A* **1953**, *89*, 522.
(61) Sandhu. *J. Magn. Reson.* **1975**, *17*, 34.
(62) Wolynes, P. G. *Annu. Rev. Phys. Chem.* **1980**, *31*, 345.
(63) Ulstrup, J. *Charge Transfer Processes in Condensed Media*; Springer: Berlin, 1979.
(64) Terazima, M.; Okamoto, K.; Hirota, N. *J. Chem. Phys.* **1995**, *102*, 2506.
(65) Zwanzig, R. *J. Chem. Phys* **1970**, *53*, 3625.
(66) Kennard, O.; Watson, D. G.; Rodgers, J. R. *Crystal Data Determinative Tables*, 3rd ed.; U.S. Department of Commerce, National Bureau of Standards, and the JCPDS-International Center for Diffraction Data: Washington, DC, 1978.
(67) Wyckoff, R. W. G. *Crystal Structures*; Interscience Publishers: New York, 1969; Vol. 6.
(68) Andersen, H. C. Personal Communication.
(69) Misawa, M.; Fukunaga, T. *J. Chem. Phys.* **1990**, *93*, 3495.
(70) Domingue, R. P.; Fayer, M. D. *J. Chem. Phys.* **1985**, *83*, 2242.
(71) Agmon, N.; Hopfield, J. J. *J. Chem. Phys.* **1983**, *78*, 6947.
(72) Pines, E.; Huppert, D.; Agmon, N. *J. Chem. Phys.* **1988**, *88*, 5620.
(73) Press, W. H.; Flannery, B. P.; Teukolsky, S. A.; Vetterling, W. T. *Numerical Recipes in C*; Cambridge University Press: Cambridge, 1988.
(74) Nelder, J. A.; Mead, R. *Comput. J.* **1965**, *7*, 308.
(75) Chapman, S.; Cowling, T. G. *The Mathematical Theory of Non-Uniform Gases*; Cambridge University Press: Cambridge, 1970.
(76) Protopapas, P.; Andersen, H. C.; Parlee, N. A. D. *Chem. Phys.* **1975**, *8*, 17.
(77) Alder, B. J.; Wainwright, T. E. *Phys. Rev. Lett.* **1967**, *18*, 988.
(78) Alder, B. J.; Gass, D. M.; Wainwright, T. E. *J. Chem. Phys.* **1970**, *53*, 3813.
(79) Czworniak, K. J.; Andersen, H. C.; Pecora, R. *Chem. Phys.* **1975**, *11*, 451.
(80) Chandler, D. *J. Chem. Phys.* **1974**, *60*, 3500.
(81) Chandler, D. *J. Chem. Phys.* **1974**, *60*, 3508.
(82) Chandler, D.; Weeks, J. D.; Andersen, H. C. *Science* **1983**, *220*, 787.
(83) Hansen, J. P.; McDonald, I. R. *Theory of Simple Liquids*; Academic Press, Inc.: London, 1976.

(84) McQuarrie, D. A. *Statistical Mechanics*; Harper & Row: New York, 1976.
(85) Narten, A. H. *J. Chem. Phys.* **1976**, *65*, 573.
(86) Lowden, L. J.; Chandler, D. *J. Chem. Phys.* **1974**, *61*, 5228.
(87) Schulten, Z.; Schulten, K. *J. Chem. Phys.* **1977**, *66*, 4616.
(88) Schulten, K.; Wolynes, P. G. *J. Chem. Phys.* **1978**, *68*, 3292.
(89) Debye, P. *Polar Molecules*; Dover: New York, 1929.
(90) Mozumder, A. *J. Chem. Phys.* **1969**, *50*, 3153.
(91) Moog, R. S.; Ediger, M. D.; Boxer, S. G.; Fayer, M. D. *J. Phys. Chem.* **1982**, *86*, 4694.
(92) Pinnow, D. A.; Candau, S. J.; Litovitz, T. A. *J. Chem. Phys.* **1968**, *49*, 347.
(93) Barbara, P. F.; Jarzeba, W. *Adv. Photochem.* **1990**, *15*, 1.
(94) Castner, E. W.; Fleming, G. R.; Bagchi, B.; Maroncelli, M. *J. Chem. Phys.* **1988**, *89*, 3519.
(95) Kahlow, M. A.; Jarzeba, W.; Kang, T. J.; Barbara, P. F. *J. Chem. Phys.* **1990**, *90*, 151.
(96) Weaver, M. J.; McManis, G. E.; Jarzeba, W.; Barbara, P. F. *J. Phys. Chem.* **1990**, *94*, 1715.
(97) Castner, E. W.; Marconcelli, M.; Fleming, G. R. *J. Chem. Phys.* **1987**, *86*, 1090.
(98) Maroncelli, M.; MacInnis, J.; Fleming, G. R. *Science* **1989**, *243*, 1674.
(99) Closs, G. L.; Miller, J. R. *Science* **1988**, *240*, 440.
(100) Connolly, J. S.; Bolton, J. R. In *Photoinduced Electron Transfer*; Fox, M. A., Chanon, M., Eds.; Elsevier: New York, 1989; Vol. D; pp 303−393.
(101) Hynes, J. T. In *Ultrafast Dynamics of Chemical Systems*; Simon, J. D., Ed.; Kluwer: Dordrecht, 1994; p 345.
(102) Sumi, H.; Marcus, R. A. *J. Chem. Phys.* **1986**, *84*, 4894.
(103) Rips, I.; Jortner, J. *J. Chem. Phys.* **1987**, *87*, 6513.
(104) Tachiya, M.; Hilczer, M. In *Ultrafast Reaction Dynamics and Solvent Effects*; Gauduel, Y., Rossky, P. J., Eds.; AIP Press: New York, 1994; p 447.
(105) Rasaiah, J. C.; Zhu, J. In *Ultrafast Reaction Dynamics and Solvent Effects*; Gauduel, Y., Rossky, P. J., Eds.; AIP Press: New York, 1994; p 421.
(106) Cave, R. J.; Newton, M. D.; Kumar, K.; Zimmt, M. B. *J. Phys. Chem.* **1995**, *99*, 17501.